Supporting Information

One-pot synthesis of O-doped BN nanosheets as capacitive deionization electrode for efficient removal of heavy metal ions from water

Ming Ming Chen, [a,b] Da Wei, [a,b] Wei Chu, [c] Tao Wang [a,b] and Dong Ge Tong [a,b*]

[a] State Key Laboratory of Geohazard Prevention and Geoenvironment Protection, Chengdu University of Technology, Chengdu 610059, China. E-mail: tongdongge@163.com; Fax: +86 28 8407 3193

[b] Collaborative Innovation Center of Panxi Strategic Mineral Resources Multi-purpose Utilization, College of Materials and Chemistry & Chemical Engineering, Chengdu University of Technology, Chengdu 610059, China.

[c] School of Chemical Engineering & Institute of New Energy and Low Carbon Technology, Sichuan University, Chengdu 610065, China. E-mail: chuwei1965@foxmail.com; Fax: +86 28 8540 3397

Summary: 41 Pages; 10 Tables; 32 Figures

Table of Contents

Table S1 The effect of reaction parameters, including reaction temperature, reaction time, NOCl/CuB_{23} nanosheets, ionic liquid volume and ionic liquid kinds on the yields, average thickness, and chemical composition of BNO nanosheets

Sample	Reaction temperature/ ºC	Reaction time /min	NOCl/CuB_{23} nanosheets	Ionics liquid volume/ml	Ionics liquid kinds	Yields /%	Nanosheets yields /%	Average thickness /nm	Chemical composition
1	25	30	25:1	50	[BMIM]Cl	100.0	100.0	1.033	BNO
2	35	24	25:1	50	[BMIM]Cl	100.0	100.0	1.033	BNO
3	45	19	25:1	50	[BMIM]Cl	100.0	100.0	1.033	BNO
4	55	14	25:1	50	[BMIM]Cl	100.0	100.0	1.033	BNO
5	65	10	25:1	50	[BMIM]Cl	100.0	100.0	1.033	BNO
6	25	30	25:1	50	[BMIM]Cl	100.0	100.0	1.033	BNO
7	25	60	25:1	50	[BMIM]Cl	100.0	100.0	1.033	BNO
8	25	20	25:1	50	[BMIM]Cl	70.0	100.0	1.033	BNO
9	25	10	25:1	50	[BMIM]Cl	55.0	100.0	1.033	BNO
10	25	5	25:1	50	[BMIM]Cl	38.0	100.0	1.033	BNO
11	25	2	25:1	50	[BMIM]Cl	23.0	100.0	1.033	BNO
12	25	1	25:1	50	[BMIM]Cl	12.0	100.0	1.033	BNO
13	25	0.5	25:1	50	[BMIM]Cl	5.0	100.0	1.033	BNO
14	25	30	24:1	50	[BMIM]Cl	97.0	100.0	1.033	BNO
15	25	30	23:1	50	[BMIM]Cl	90.0	100.0	1.033	BNO
16	25	30	25:1	50	[BMIM][BF_4]	100.0	100.0	1.033	BNO
17	25	30	25:1	50	[BMIM][PF_6]	100.0	100.0	1.033	BNO
18	25	30	25:1	70	[BMIM]Cl	100.0	100.0	1.033	BNO
19	25	30	25:1	30	[BMIM]Cl	90.0	100.0	1.033	BNO

Table S2 Evaluated model parameters of the adsorption isotherms of BNO nanosheets over Cd^{2+} at 298 K

Langmuir model	**Freundlich model**
$q_m = 2281\ mgg^{-1}$	$1/n = 0.5101$
$K_L = 0.003581\ (Lmg^{-1})$	$K_F = 58.3115\ (mgg^{-1})(Lmg^{-1})^{1/n}$
$R^2 = 0.9990$	$R^2 = 0.9643$

Table S3 Cd^{2+} electrosorption dimensionless quantity (R_L) over BNO nanosheets at different initial concentrations

Initial concentrations / mgL^{-1}	**R_L**
100	0.74
200	0.58
300	0.48
400	0.41
600	0.32
800	0.26
1000	0.22
1200	0.19

Table S4 Parameters of pseudo-first-order and pseudo-second-order models for the electro-adsorption of Cd^{2+} onto BNO nanosheets at 298 K under 1.2V

Pseudo-first-order model	**Pseudo-second-order model**
C_0 = 600 mgL^{-1}	C_0 = 600 mgL^{-1}
$q_{e,\ exp}$ = 1395 mgg^{-1}	$q_{e,\ exp}$ = 1395 mgg^{-1}
$q_{e,cal}$ = 18 mgg^{-1}	$q_{e,cal}$ = 1395 mgg^{-1}
K_1= 0.1494	K_2 = 8.06×10^{-4}
R^2 = 0.9253	R^2 = 1

Table S5 Parameters of pseudo-first-order and pseudo-second-order kinetics in terms of different voltages for the electrosorption of Cd^{2+} onto BNO nanosheets at 298 K

Bias potential	**Pseudo-first-order**			**Pseudo-second-order**		
/ V	$q_{e,cal}$/ mgg^{-1}	K_1/ min^{-1}	R^2	$q_{e,cal}$ / mgg^{-1}	K_2/ gmg^{-1} min^{-1}	R^2
0	8.55	0.0758	0.9388	243	2.47×10^{-3}	0.9999
0.4	13.31	0.1035	0.8663	625	1.35×10^{-3}	0.9999
0.8	15.92	0.1200	0.9249	1000	1.00×10^{-3}	0.9999

Table S6 Thermodynamic parameters for the electrosorption of Cd^{2+} onto BNO nanosheets at 298 K

Temperature / K	**ΔG/(kJ mol^{-1})**	**ΔH/(kJ mol^{-1})**	**ΔS/(J mol^{-1})**
298 K	-2.746		
308 K	-2.222	-12.782	-33.9
318 K	-1.959		
328 K	-1.702		

Table S7 Evaluated model parameters of the electrosorption isotherms of BNO nanosheets over various cations at 298 K

Cations	**Langmuir model**			**Freundlich model**		
	q_m/ mgg^{-1}	K_L/Lg^{-1}	R^2	1/n	K_F/(mgg^{-1})(Lmg^{-1})$^{1/n}$	R^2
Pb^{2+}	735	0.00238	1	0.6399	6.85	0.9286
Cu^{2+}	858	0.00244	0.9996	0.6363	8.29	0.9274
Ni^{2+}	976	0.00250	0.9995	0.6331	9.62	0.9263
Co^{2+}	865	0.00251	0.9995	0.6328	9.77	0.9262
Zn^{2+}	3211	0.00515	0.9976	0.5331	81.22	0.8875
Mg^{2+}	829	0.00245	0.9996	0.6361	8.38	0.9273
Ca^{2+}	963	0.00243	0.9996	0.6372	7.95	0.9277
Fe^{2+}	971	0.00251	0.9995	0.6329	9.71	0.9262
Fe^{3+}	1200	0.00287	0.9998	0.5923	13.21	0.9154
Na^{+}	578	0.00203	1	0.6405	5.56	0.9213

Table S8 Parameters of pseudo-first-order and pseudo-second-order models for the electrosorption over various cations at 298 K

Cations	**C_0/mgL^{-1}**	**$q_{e,exp}$ /mgg^{-1}**	**Pseudo-first-order model**			**Pseudo-second-order model**		
			$q_{e,cal}$ /mgg^{-1}	k_1/min^{-1}	R^2	$q_{e,cal}$ /mgg^{-1}	k_2/ gmg^{-1} min^{-1}	R^2
Pb^{2+}	600	220	10.9	0.0750	0.9325	426	0.00148	1
Cu^{2+}	600	488	11.3	0.0878	0.9521	514	0.00140	1
Ni^{2+}	600	559	12.3	0.0976	0.9307	580	0.00135	1
Co^{2+}	600	410	12.3	0.109	0.9558	588	0.00152	1
Zn^{2+}	600	2080	21.9	0.225	0.9179	2192	0.000693	1
Mg^{2+}	600	245	11.7	0.107	0.9299	518	0.00169	1
Ca^{2+}	600	552	11.2	0.0805	0.9600	496	0.00135	1
Fe^{2+}	600	555	12.3	0.102	0.9303	585	0.00139	1
Fe^{3+}	600	682	13.6	0.115	0.9305	680	0.001125	1
Na^{+}	600	380	10.0	0.0698	0.9211	380	0.00155	1

Table S9 Comparison of the parameters of metal ions

Ions	Charge size	Hydrated radius (Å)	Ionic radius (Å)	electronegativity	Atomic weight
Zn^{2+}	2	4.19	0.72	1.9	63.55
Cd^{2+}	2	4.26	0.97	1.69	112.4
Pb^{2+}	2	4.01	1.32	2.33	207.2
Ni^{2+}	2	4.04	0.70	1.91	58.69
Co^{2+}	2	4.23	0.72	1.88	58.93
Cu^{2+}	2	4.30	0.74	1.65	65.39
Mg^{2+}	2	4.28	0.65	1.31	24.31
Ca^{2+}	2	4.12	0.99	1.00	40.08
Fe^{2+}	2	4.28	0.75	1.83	55.85
Fe^{3+}	3	4.57	0.60	1.83	55.85
Na^{+}	1	3.58	0.98	0.90	22.99

Table S10 Fitted EIS parameters of the as-prepared BNO nanosheets in different ion solutions at room temperature.

Solutions	R_s / Ω	R_{ct} / Ω	Warburg coefficient of metal ions / $s^{1/2}cm^{-1}$
$ZnCl_2$	1.4	0.8	4.08×10^{7}
$CdCl_2$	2.1	1.1	4.52×10^{7}
$FeCl_3$	0.9	2.2	8.88×10^{7}
$NiCl_2$	1.4	2.6	9.80×10^{7}
$FeCl_2$	1.0	2.7	1.31×10^{8}
$CaCl_2$	1.3	2.8	1.92×10^{8}
$CuCl_2$	1.1	3.1	2.69×10^{8}
$CoCl_2$	1.0	3.7	3.96×10^{8}
NaCl	1.2	4.0	5.02×10^{8}
$MgCl_2$	1.2	6.2	6.77×10^{8}
$PbCl_2$	1.5	6.9	7.61×10^{8}

R_s represents for the electrolyte resistance and R_{ct} for the charge transfer resistance.

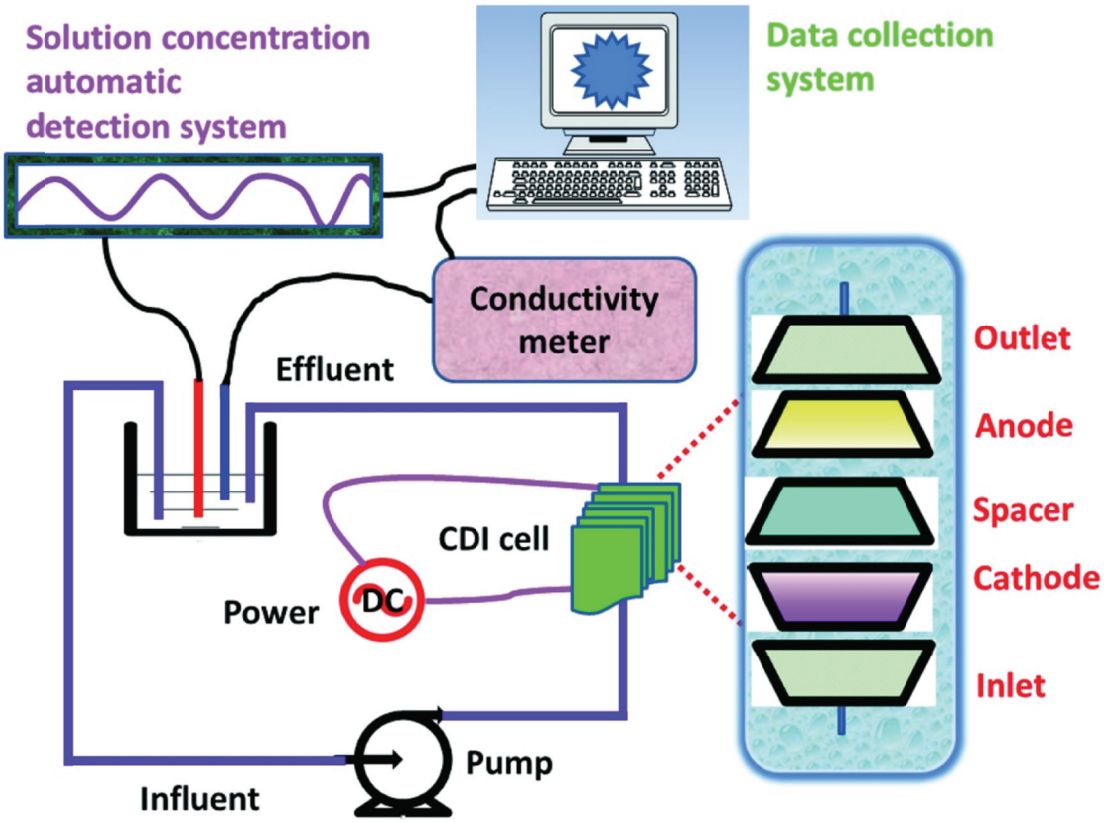

Fig.S1 Schematic diagram for the CDI cell set-up in our work.

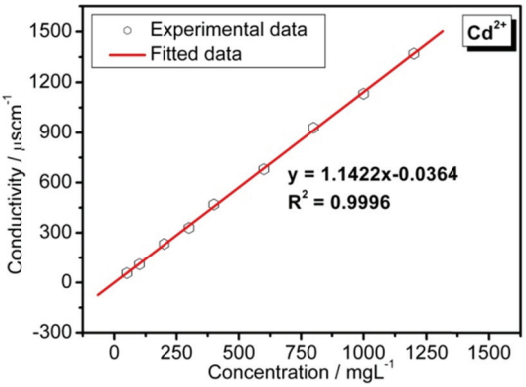
Experimental data
Fitted data
Cd2+
y = 1.1422x-0.0364
R2 = 0.9996
Conductivity / µscm-1
Concentration / mgL-1

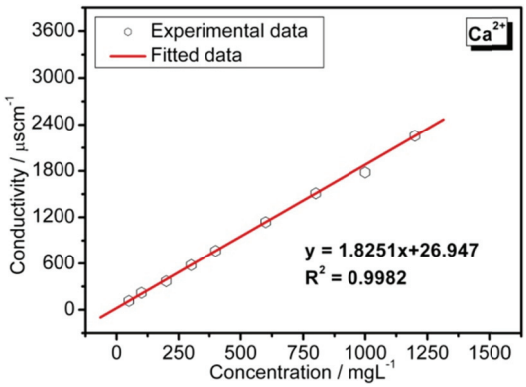
Experimental data
Fitted data
Ca2+
y = 1.8251x+26.947
R2 = 0.9982
Conductivity / µscm-1
Concentration / mgL-1

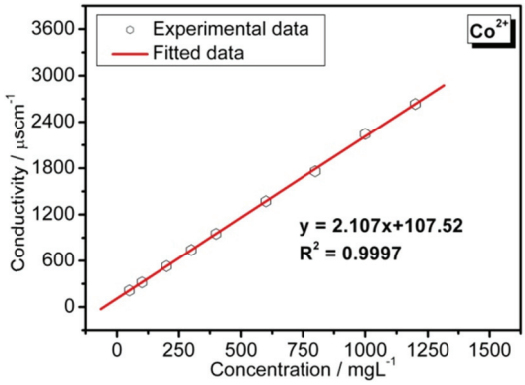
Experimental data
Fitted data
Co2+
y = 2.107x+107.52
R2 = 0.9997
Conductivity / µscm-1
Concentration / mgL-1

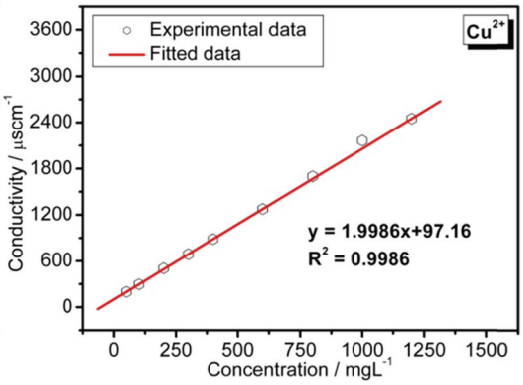
Experimental data
Fitted data
Cu2+
y = 1.9986x+97.16
R2 = 0.9986
Conductivity / µscm-1
Concentration / mgL-1

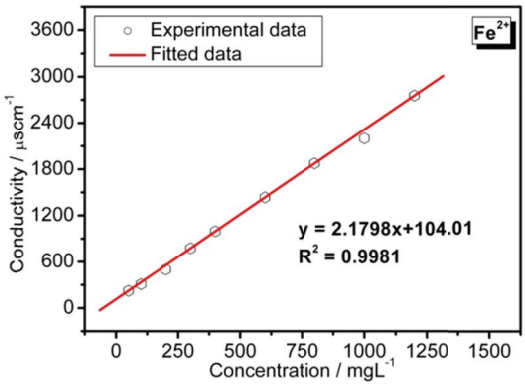
Experimental data
Fitted data
Fe2+
y = 2.1798x+104.01
R2 = 0.9981
Conductivity / µscm-1
Concentration / mgL-1

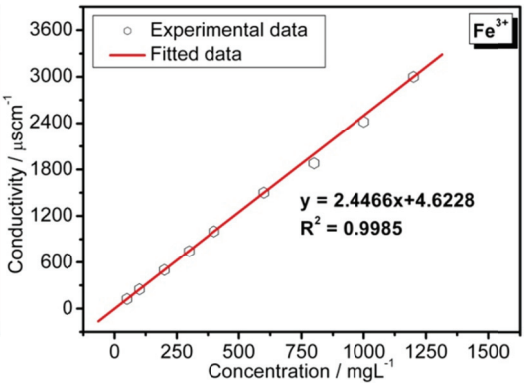
Experimental data
Fitted data
Fe3+
y = 2.4466x+4.6228
R2 = 0.9985
Conductivity / µscm-1
Concentration / mgL-1

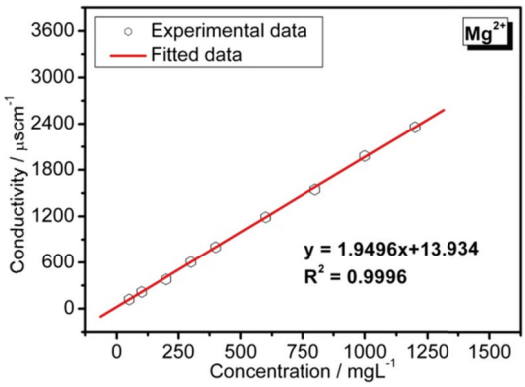
Experimental data
Fitted data
Mg2+
y = 1.9496x+13.934
R2 = 0.9996
Conductivity / µscm-1
Concentration / mgL-1

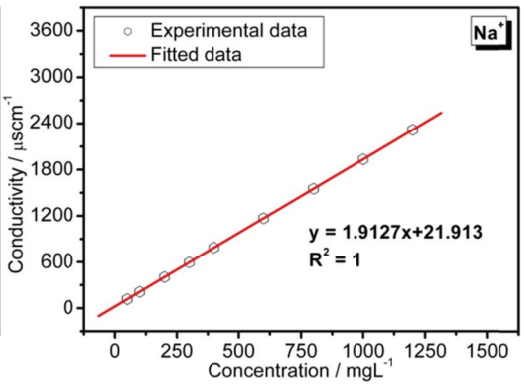
Experimental data
Fitted data
Na+
y = 1.9127x+21.913
R2 = 1
Conductivity / µscm-1
Concentration / mgL-1

(Continued)

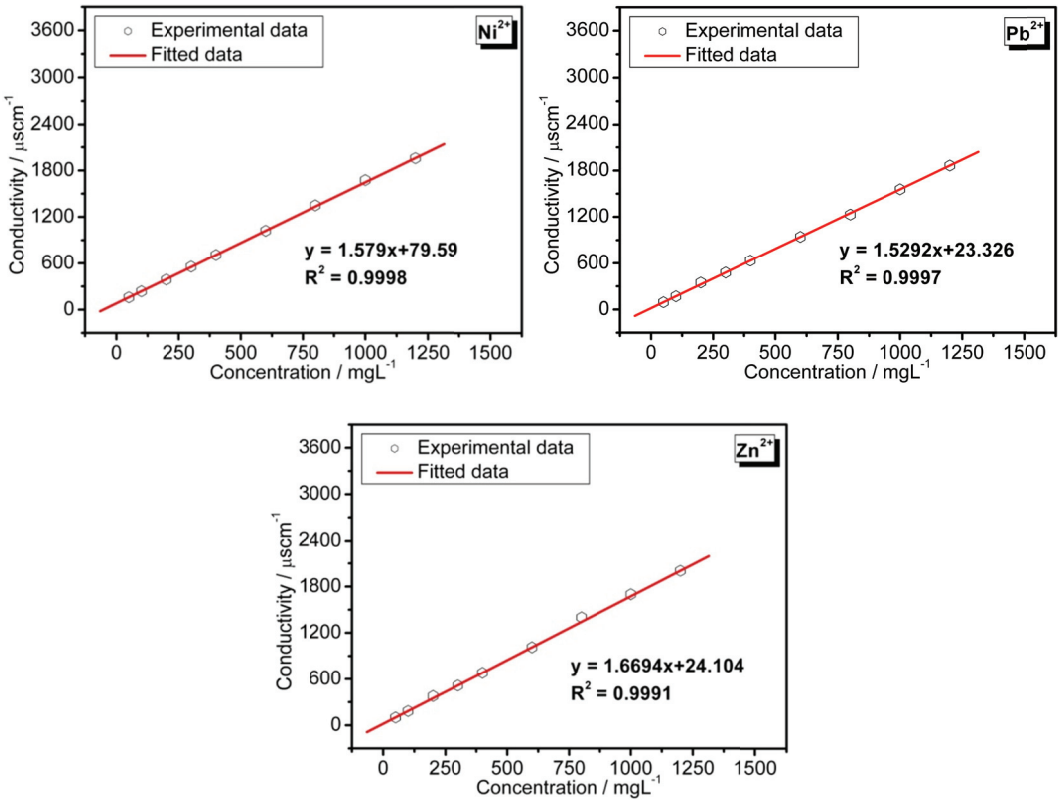

Fig.S2 The relationship between solution concentration and conductivity of various metal chloride solution.

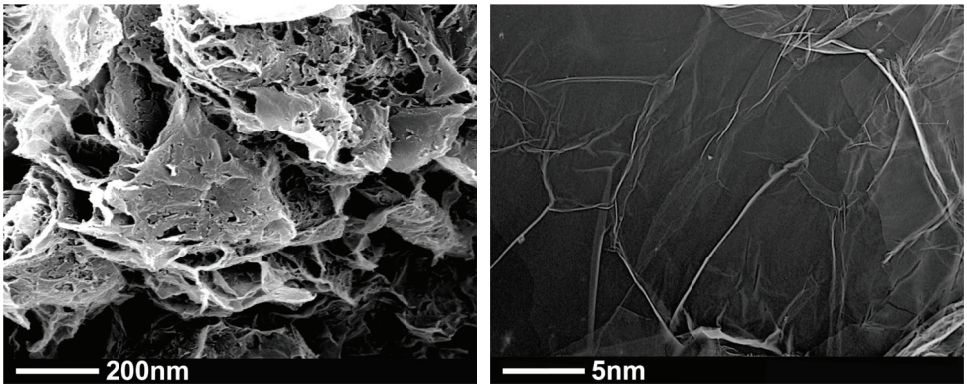

a **b**

Fig.S3 (a) Low magnification and (b) enlarged STEM images of the graphene-like CuB_{23} nanosheets.

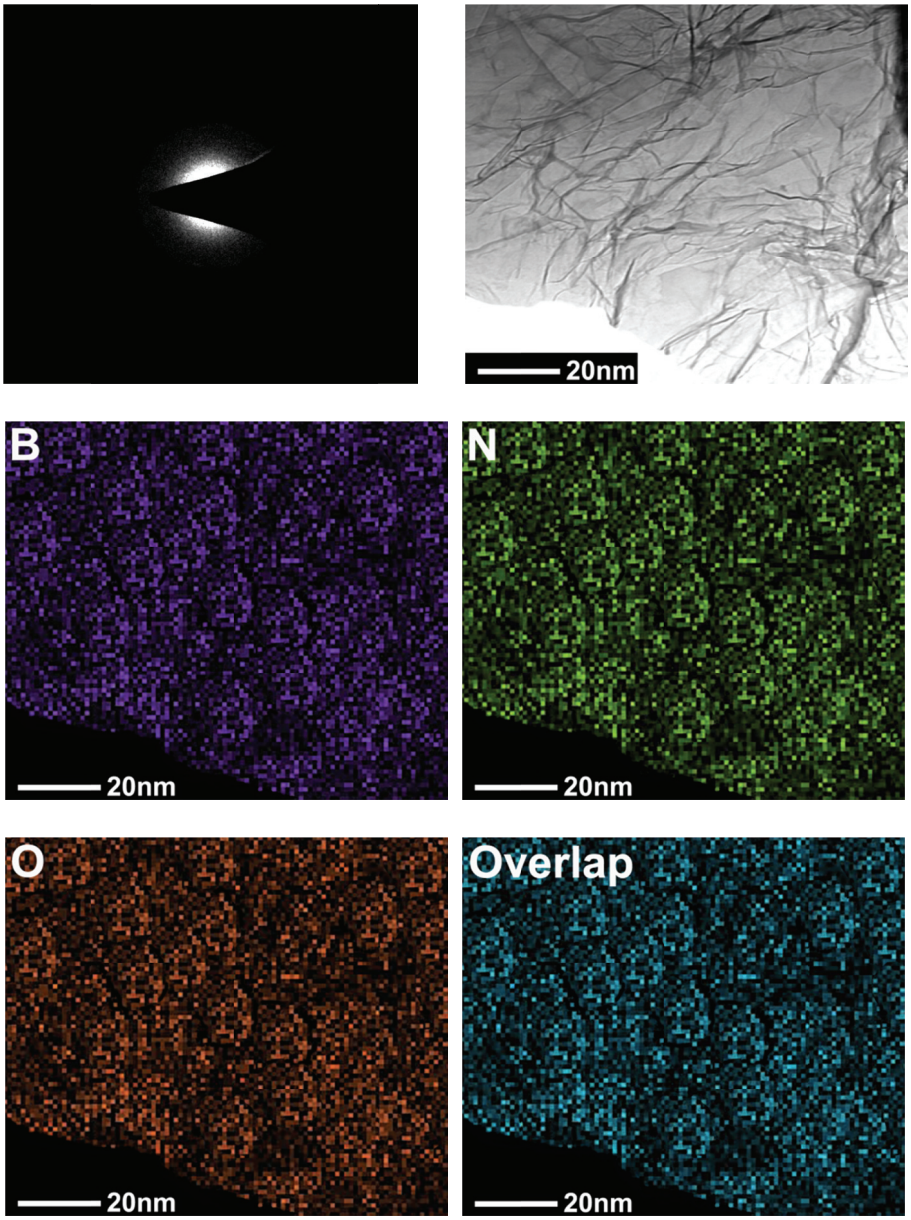

Fig.S4 SAED pattern, B, N and O elemental maps for the as-prepared BNO nanosheets of the as-prepared BNO nanosheets.

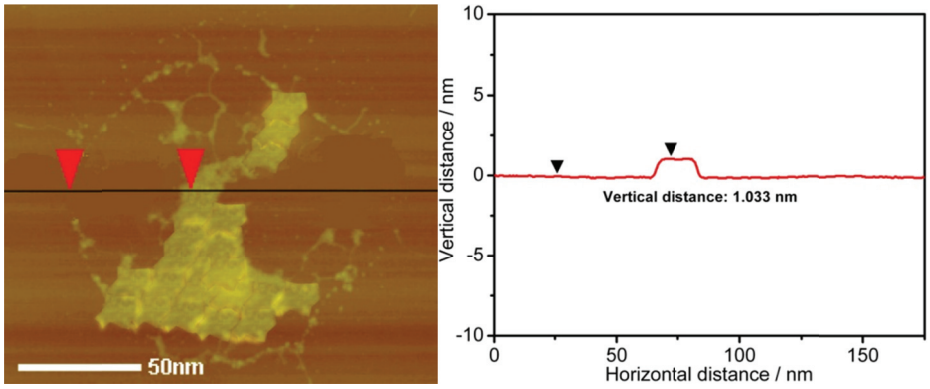

a **b**

Fig.S5 (a) AFM image and (b) the cross section analysis for the as-prepared BNO nanosheets.

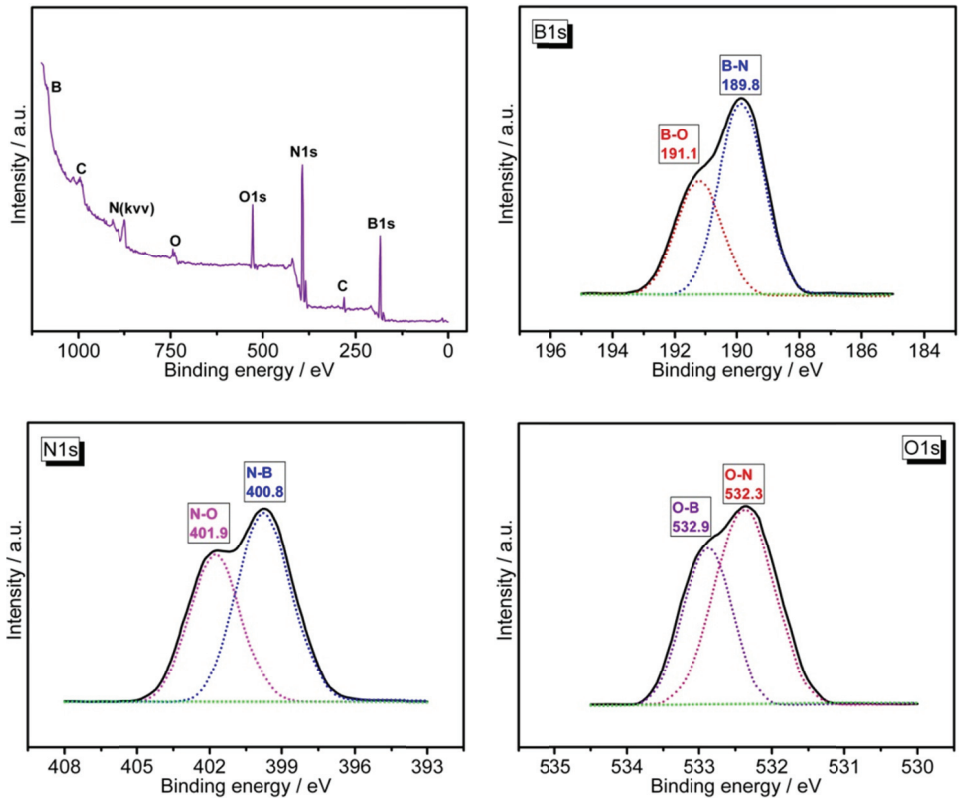

Fig.S6 XPS survey spectrum, B 1s spectra, N 1s spectra and O 1s spectra of the as-prepared BNO nanosheets.

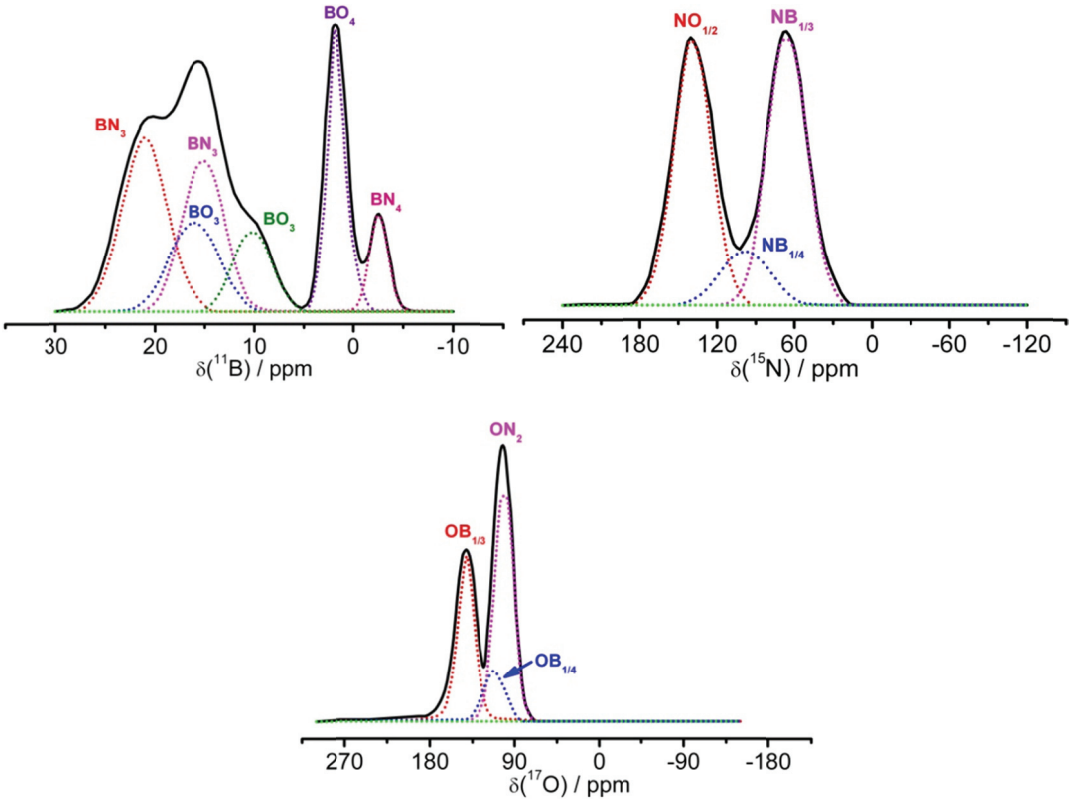

Fig.S7 ^{11}B, ^{15}N 1s and ^{17}O MAS NMR spectra of the as-prepared BNO nanosheets.

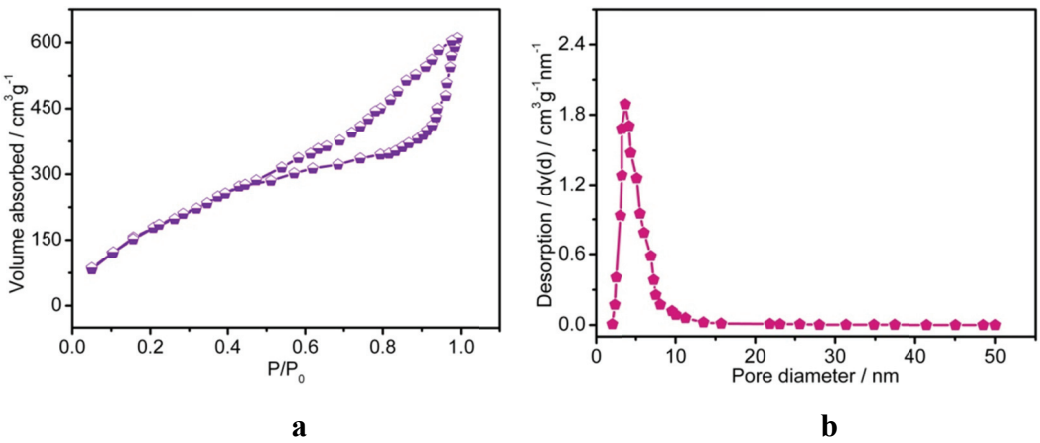

Fig.S8 (a) N_2 adsorption–desorption plots and (b) pore size distribution of the as-prepared BNO nanosheets.

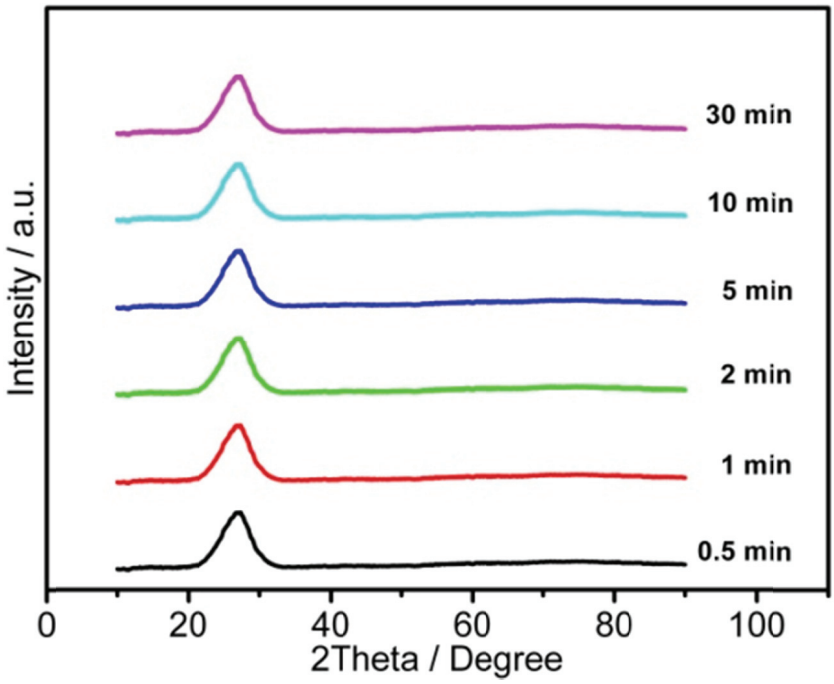

a

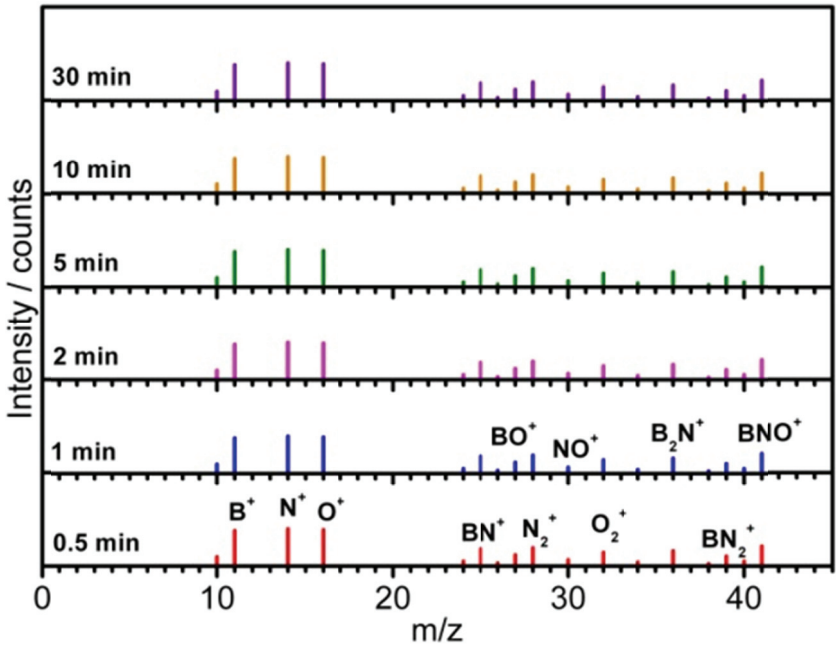

b

Fig.S9 (a) XRD patterns and (b) ToF-SIMS spectra of the products during the fabrication.

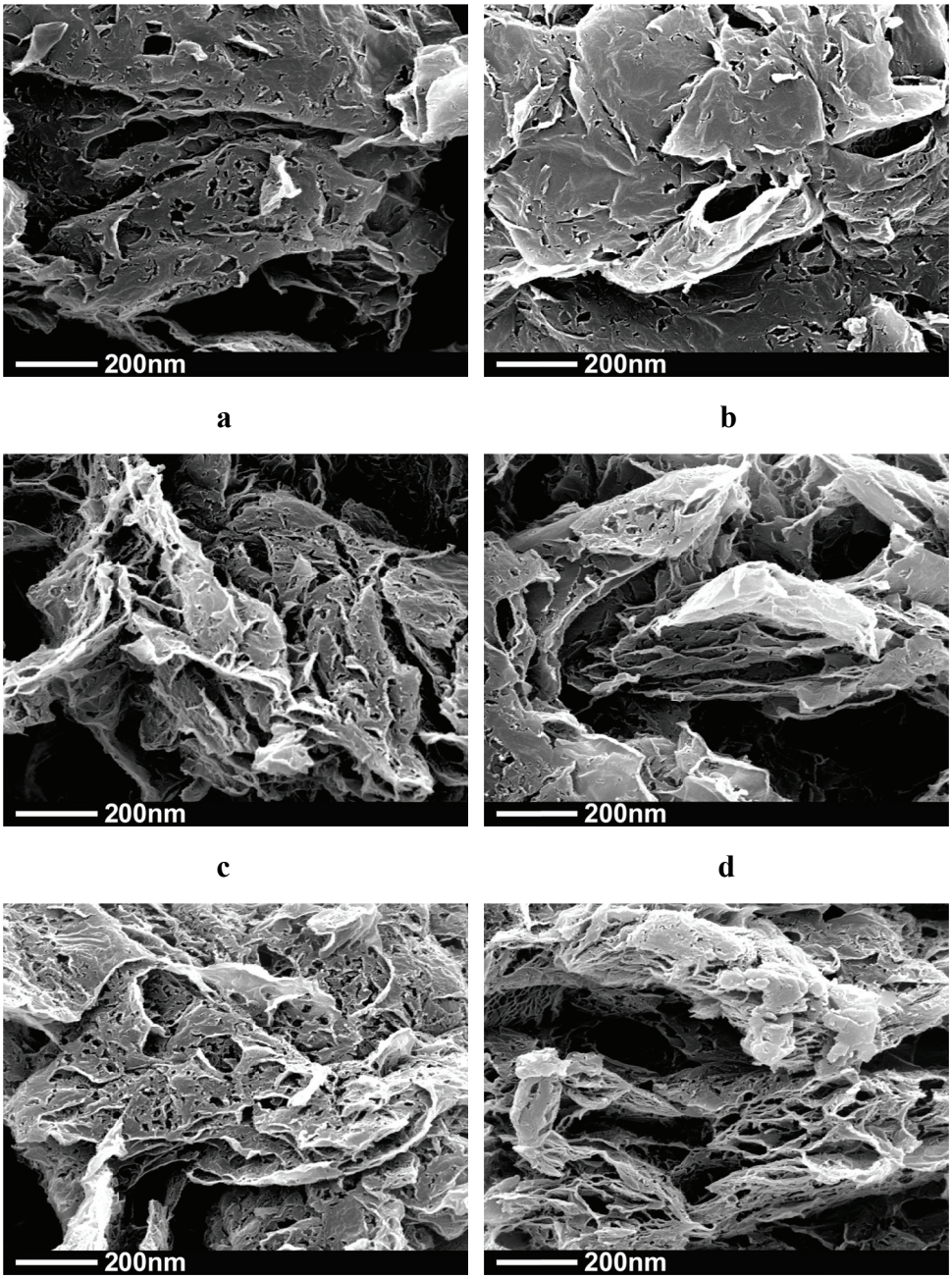

Fig.S10 STEM images of the products during the fabrication: (a) 0.5 min; (b) 1 min; (c) 2 min;(d) 5 min;(e)10 min;(f) 30 min

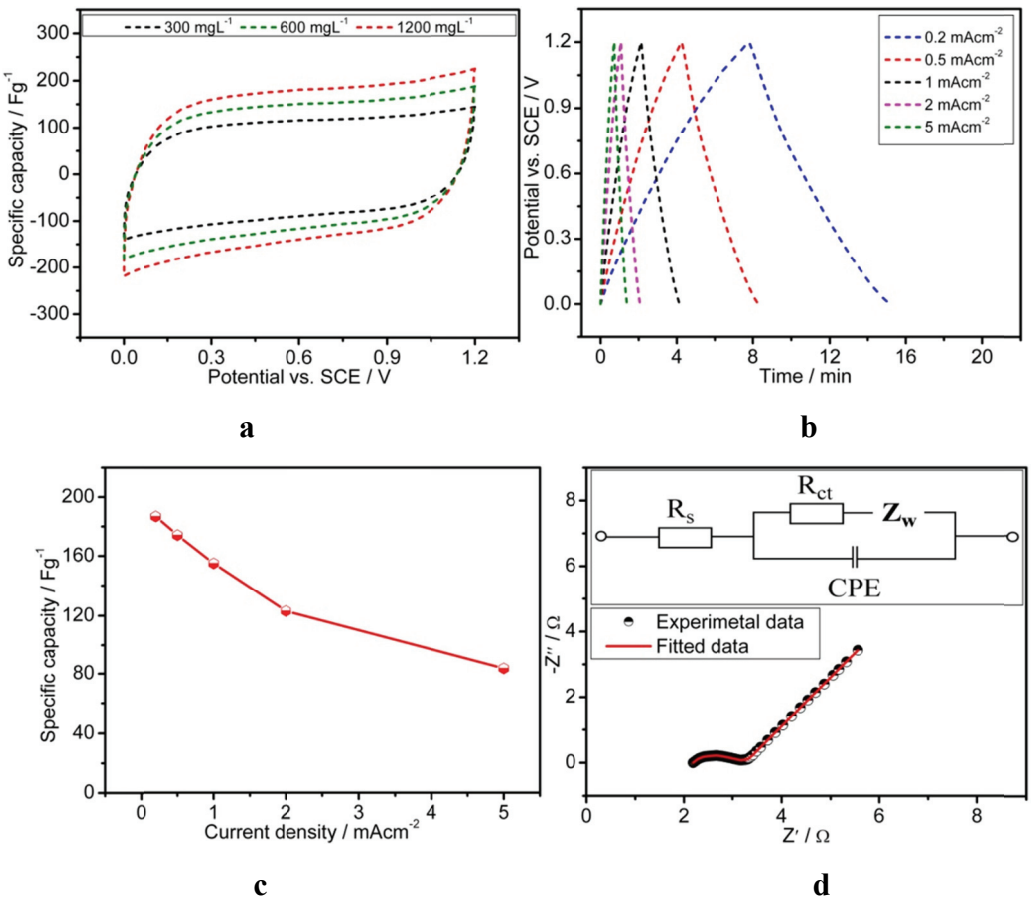

Fig.S11 (a) CV curves with different concentrations at 5 mVs^{-1}; (b) Charge/discharge curves in 600mgL^{-1} $CdCl_2$ aqueous solution at 0.2$mAcm^{-2}$; (c) Specific capacity at various diffident current density; (d) Nyquist plots and equivalent circuit (inset) in 600mgL^{-1} $CdCl_2$ aqueous solution of the as-prepared BNO nanosheets.

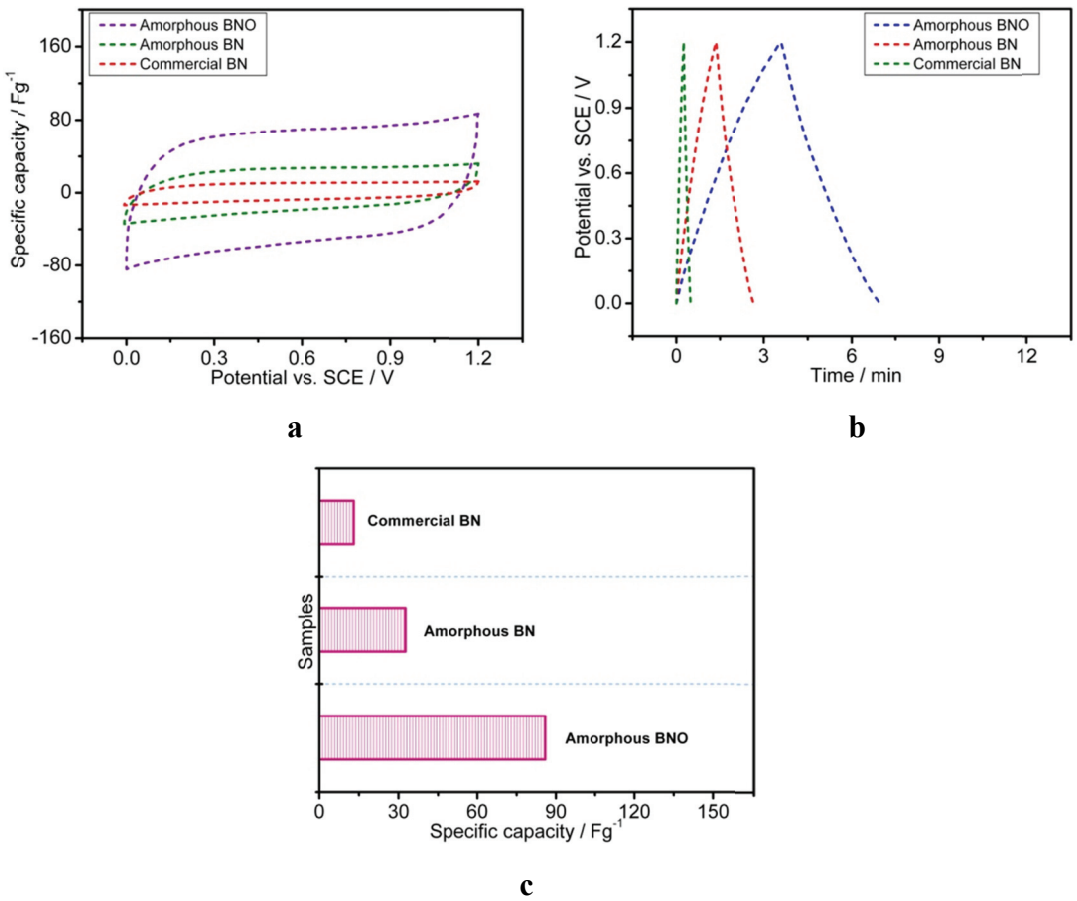

Fig.S12 (a) CV curves at 5 mVs^{-1} in 600mgL^{-1} $CdCl_2$ aqueous solution; (b) Charge-discharge profiles at 0.2 $mAcm^{-2}$ in 600mgL^{-1} $CdCl_2$ aqueous solution; (c) Specific capacity at 0.2 $mAcm^{-2}$ in 600mgL^{-1} $CdCl_2$ aqueous solution for amorphous BNO prepared in this work, commercial amorphous BN and BN.

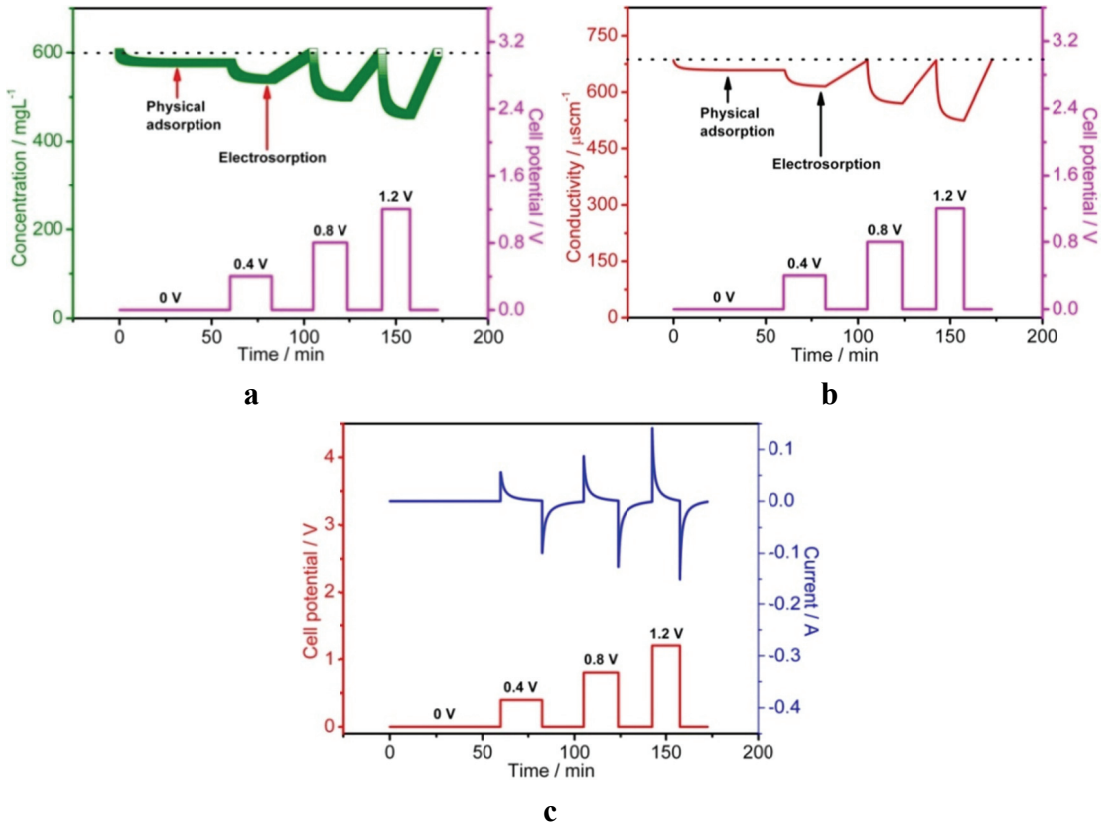

Fig.S13 (a) Solution concentration changes; (b) solution conductivity changes and (c) current signal changes for the as-prepared BNO nanosheets over 600mgL^{-1} $CdCl_2$ solution with a flowing rate of 50 mgL^{-1} at various voltages during electrosorption.

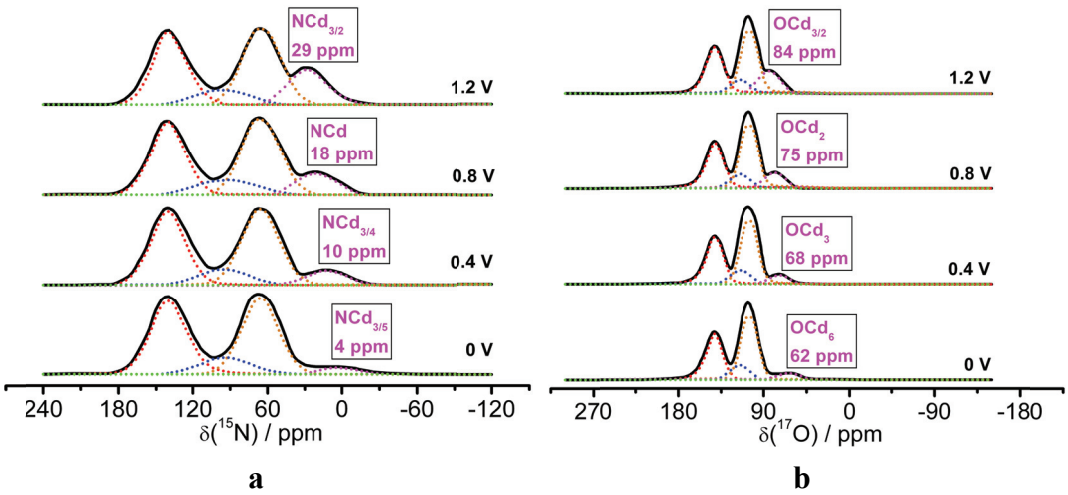

Fig.S14 (a) ^{15}Nand (b) ^{17}O MAS NMR of the charged BNO nanosheets at various voltage in $CdCl_2$ solution.

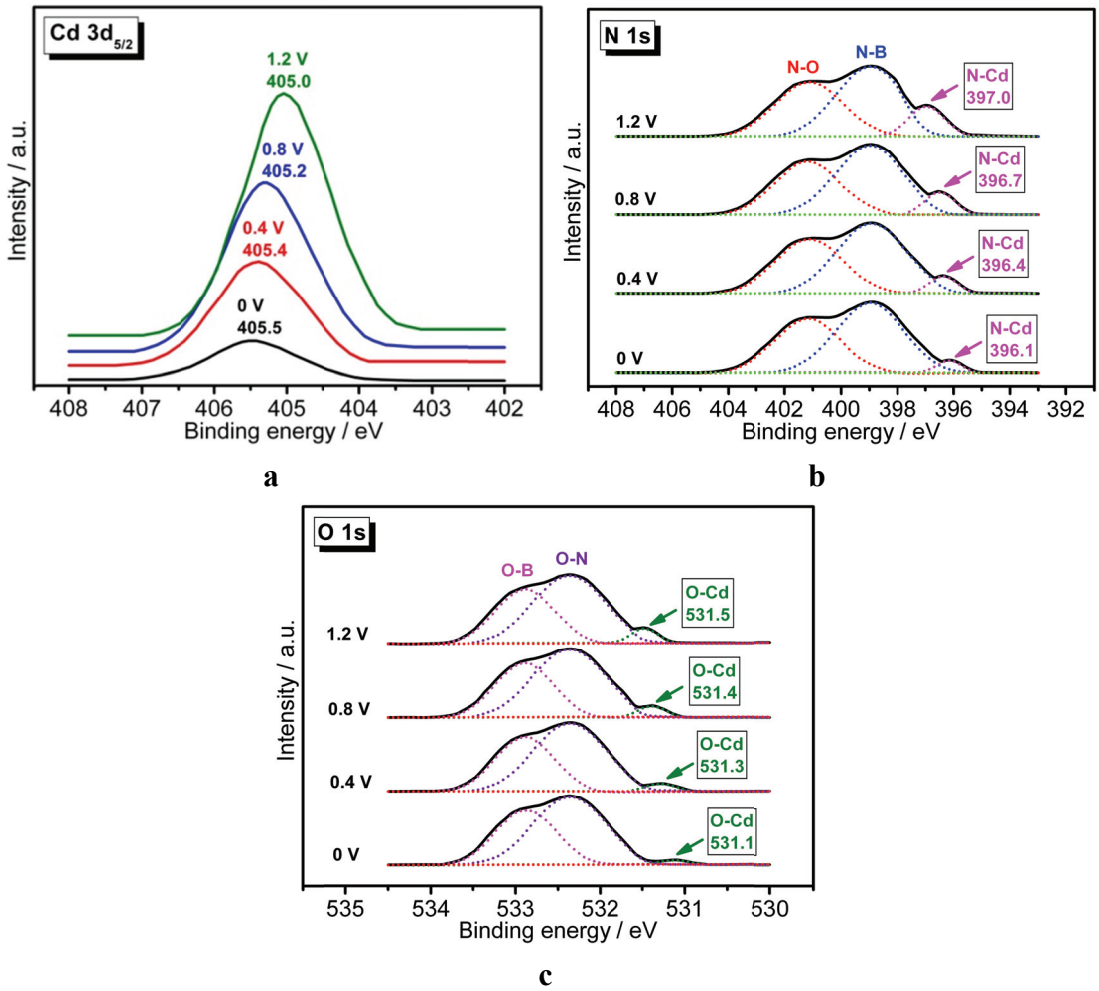

Fig.S15 (a) Cd $3d_{5/2}$ (b) N1s and (c) O1s XPS spectra of the charged BNO nanosheets at various applied voltage.

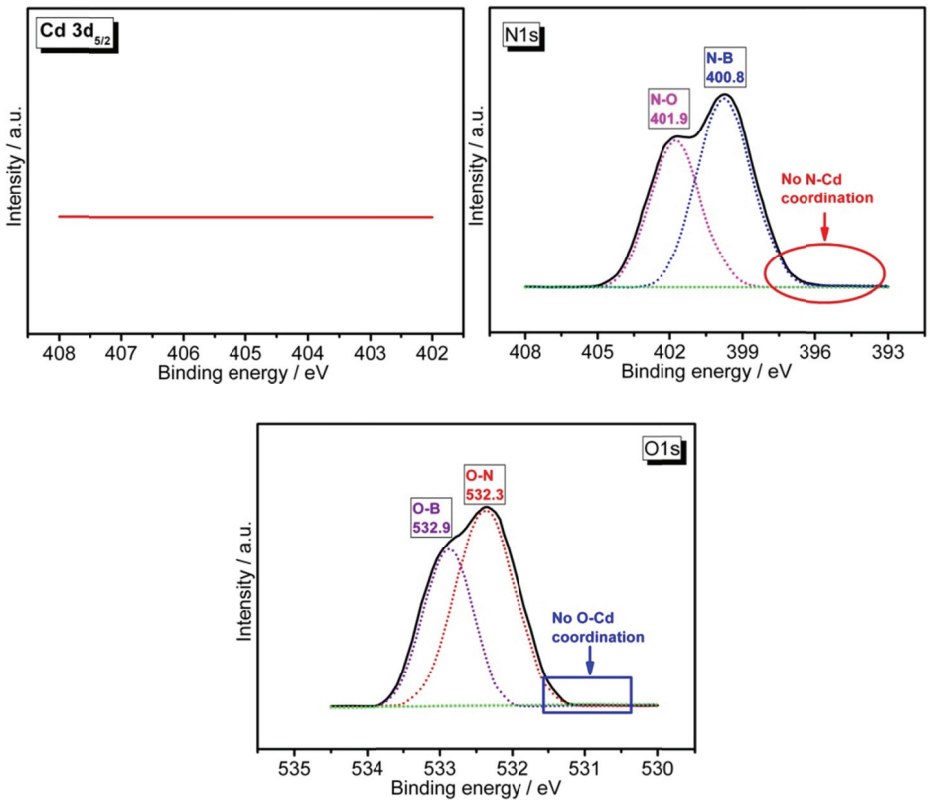

Fig.S16 Cd $3d_{5/2}$, N1s and O1s XPS spectra of the charged BNO nanosheets when the electrode was short-circuited.

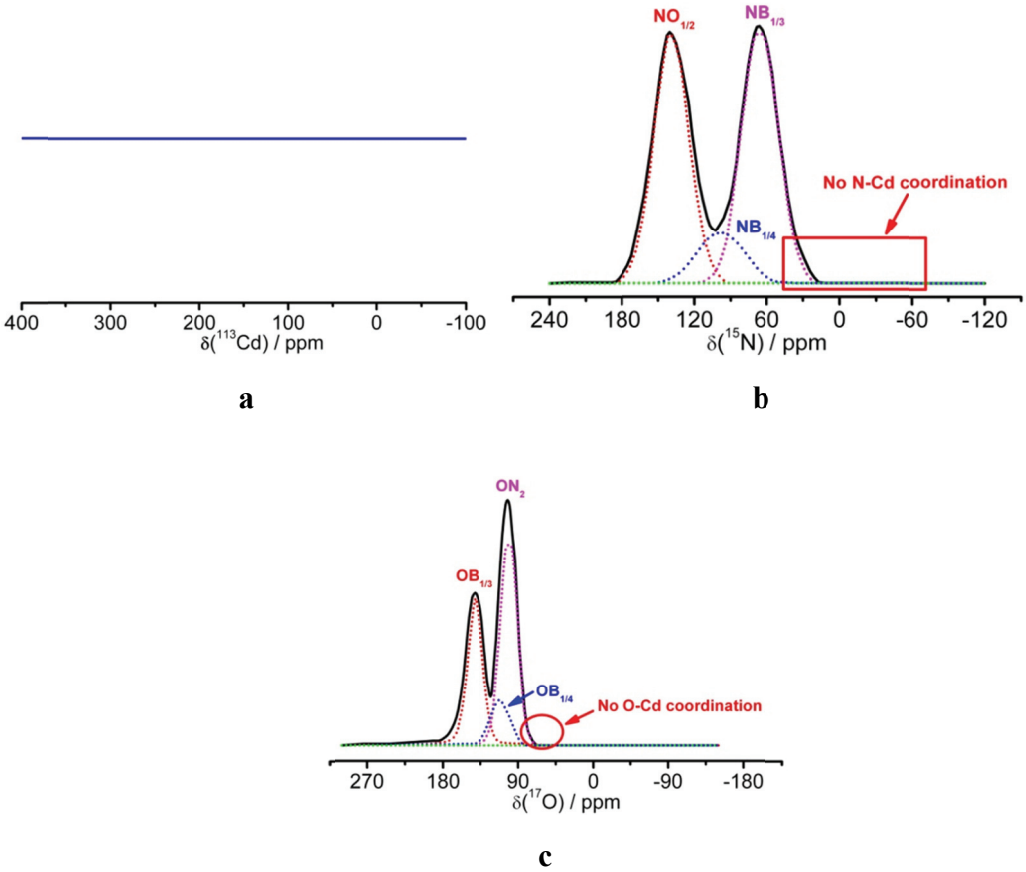

Fig.S17 (a) ^{113}Cd; (b) ^{15}N 1s and (c) ^{17}O MAS NMR spectra of the charged BNO nanosheets when the electrode was short-circuited.

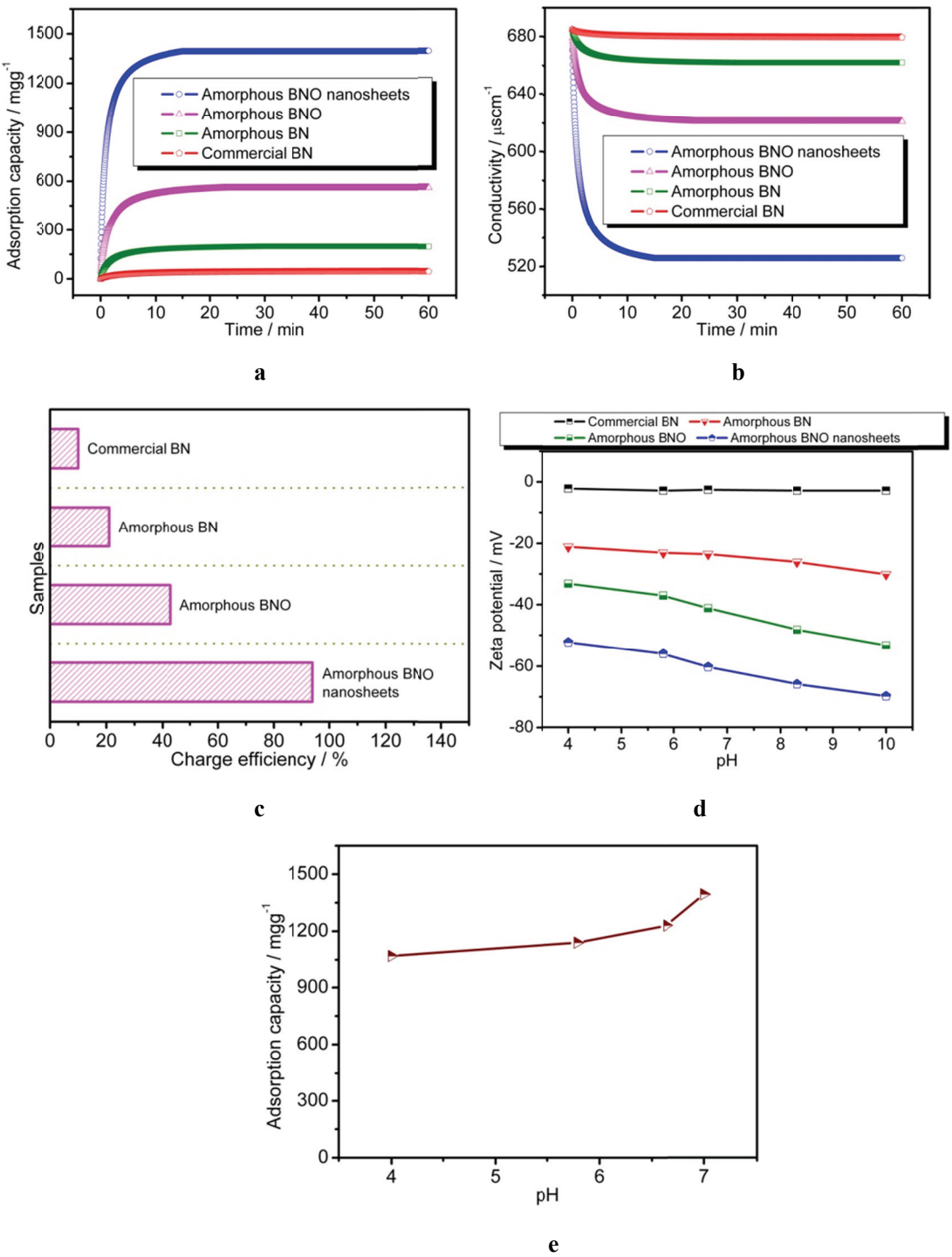

Fig.S18 (a) Electrosorption capacity vs. time profiles; (b) Solution conductivity vs. time profiles; (c) Charge efficiency and (d) Zeta potential vs. pH profiles of amorphous BNO nanosheets, amorphous BNO, commercial amorphous BN and BN, respectively; (e) The electrosorption capacity of our amorphous BNO nanosheets towards Cd^{2+} vs. pH profile at 1.2 V by CDI with a flowing rate of 50 mgL^{-1}.

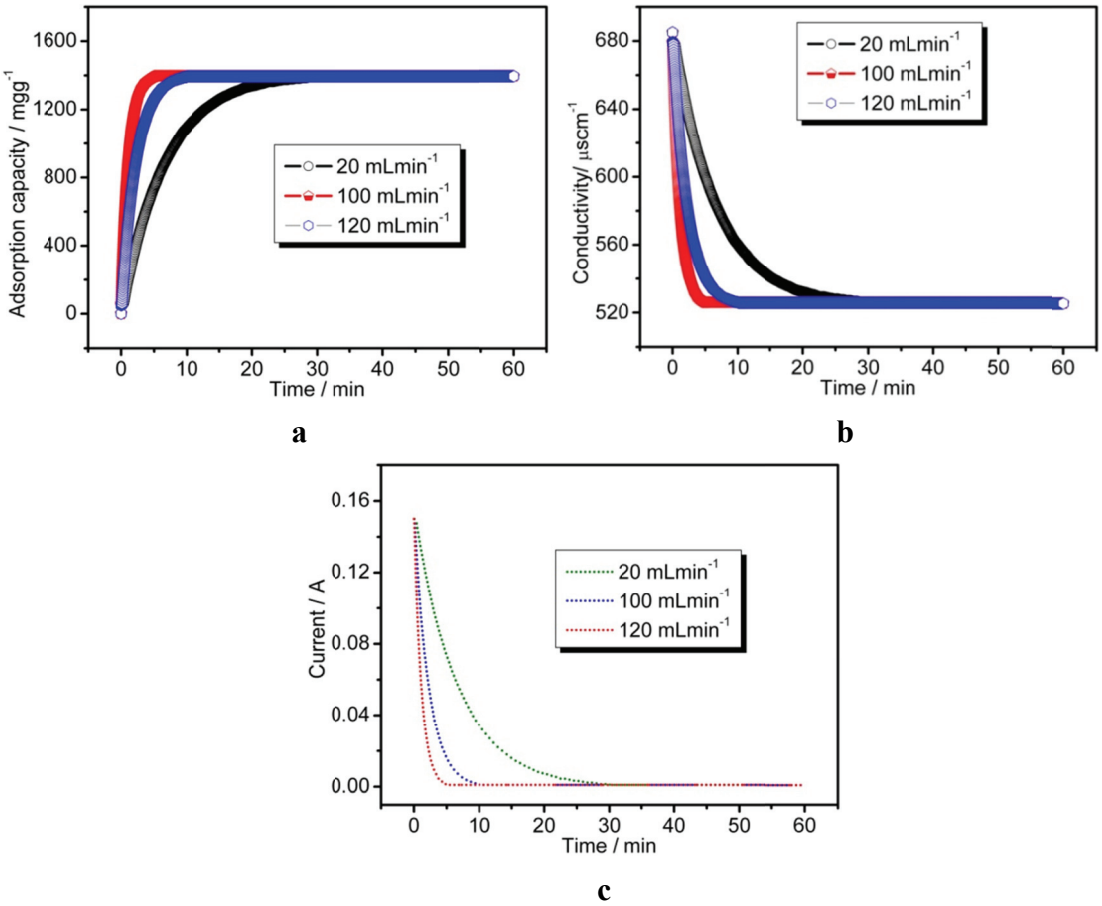

Fig.S19 (a) Electrosorption capacity; (b) Solution conductivity and (c) I-t relationships of our amorphous BNO nanosheets towards Cd^{2+} at different flowing rates during electrosorption.

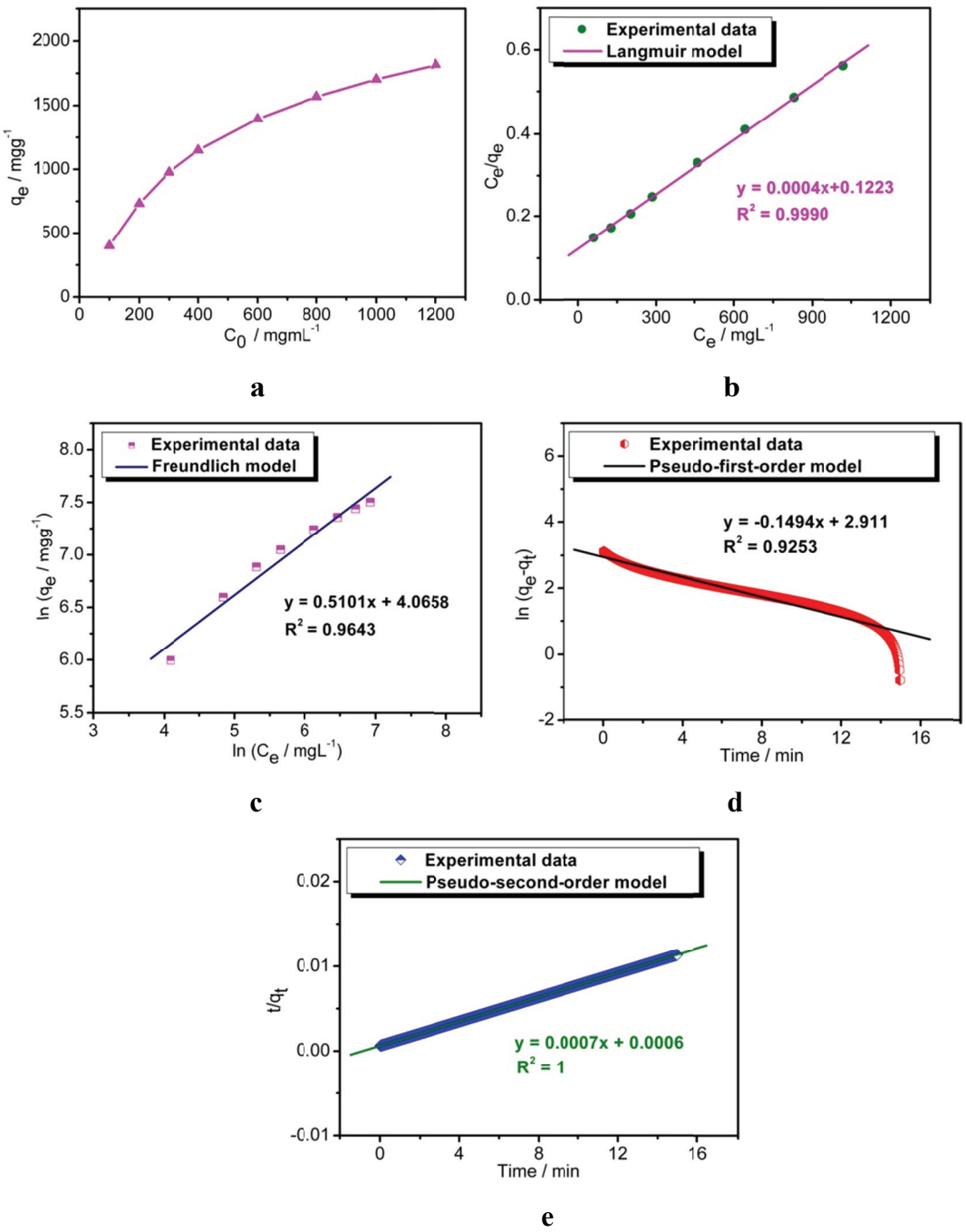

Fig.S20 (a) Electrosorption isotherm;(b) Langmuir model simulation; (c) Freundlich model simulation; (d) pseudo-first-order kinetics simulation; (e) pseudo-second-order kinetics simulation for the as-prepared BNO nanosheets over 600mgL^{-1} $CdCl_2$ aqueous solution at 1.2 V by CDI with a flowing rate of 50 mgL^{-1}.

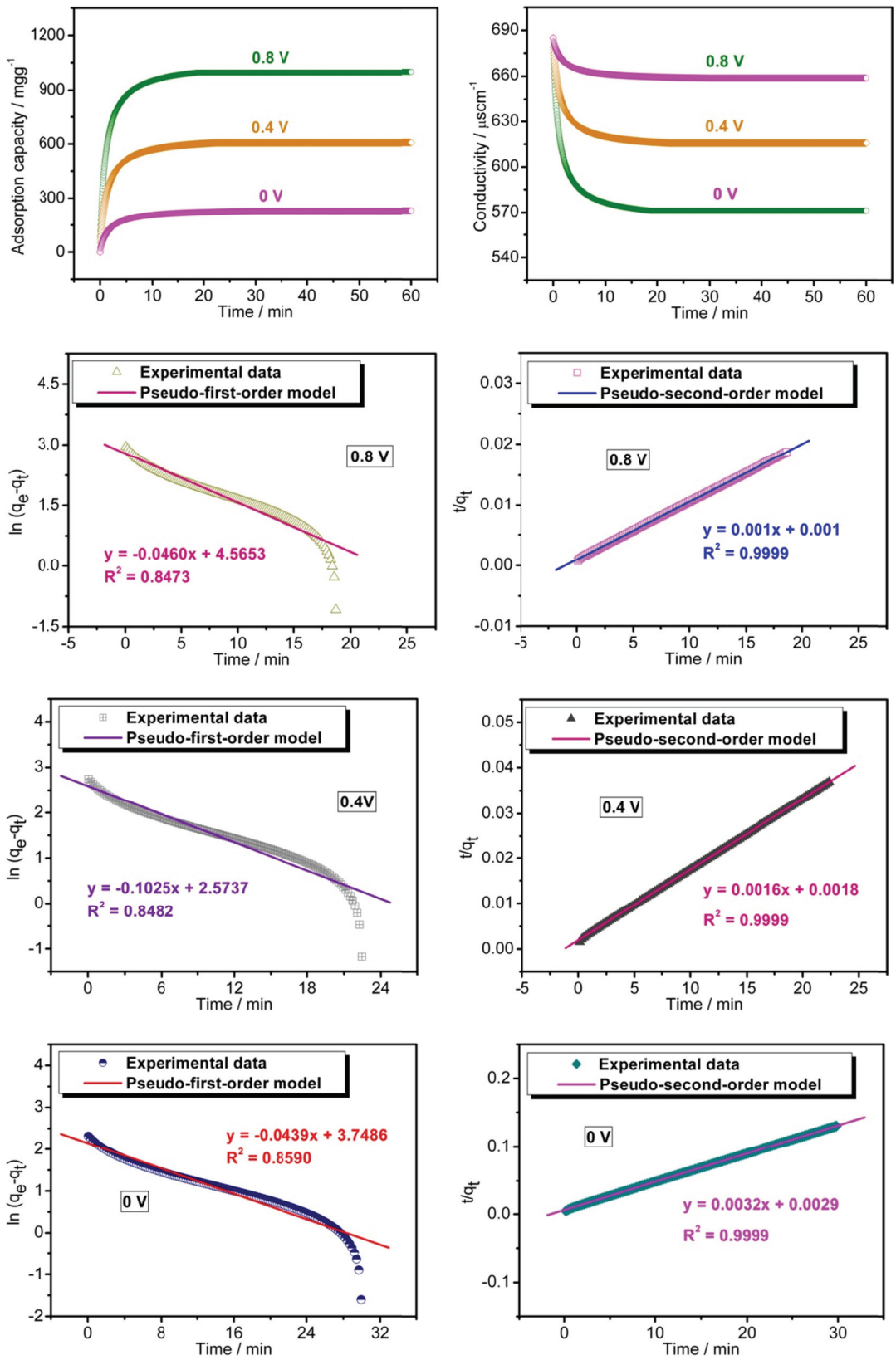

Fig.S21 (a) Electrosorption isotherm;(b) Solution conductivity; (c) Freundlich model simulation; (d) pseudo-first-order kinetics simulation; (e) pseudo-second-order

kinetics simulation for the as-prepared BNO nanosheets towards 600 mgL^{-1} $CdCl_2$ aqueous solution at different Bias potentials with a flowing rate of 50 mgL^{-1}.

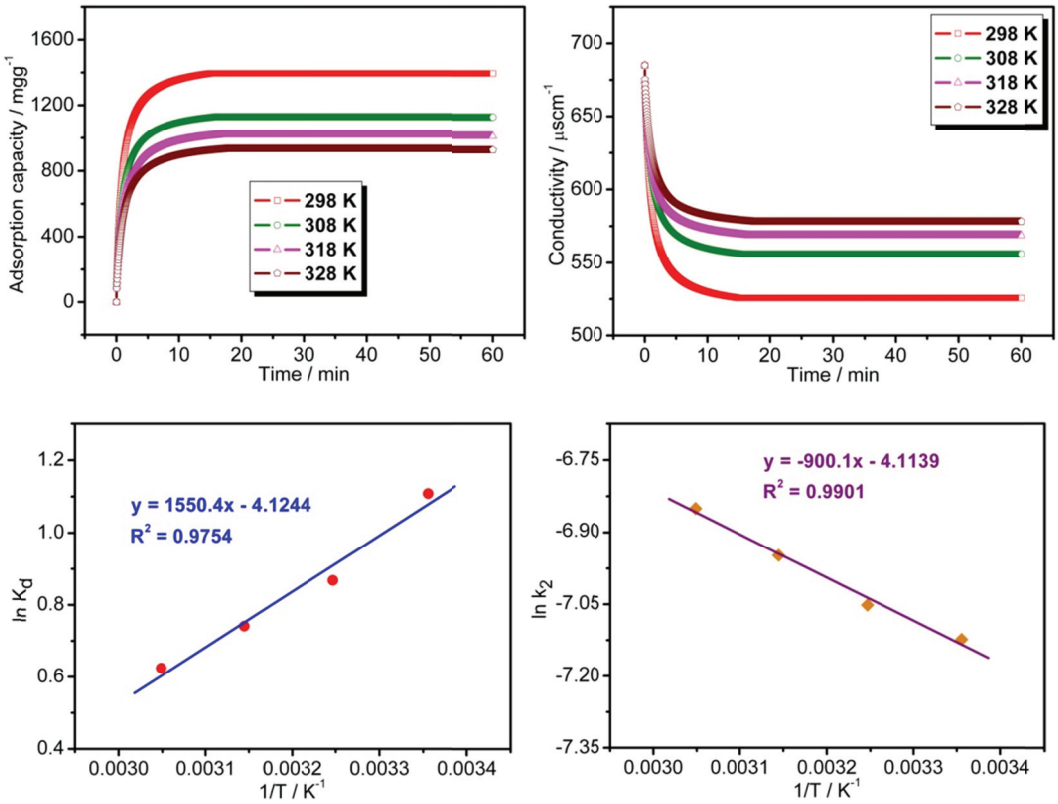

Fig.S22 (a) electro-adsorption capacity at different temperatures; (b) solution conductivity changes; (c) Plots of lnKd vs T^{-1}; (d) Plots of lnk_2 vs T^{-1} for the as-prepared BNO nanosheets towards 600 mgL^{-1} $CdCl_2$ aqueous solution at different Bias potentials with a flowing rate of 50 mgL^{-1}.

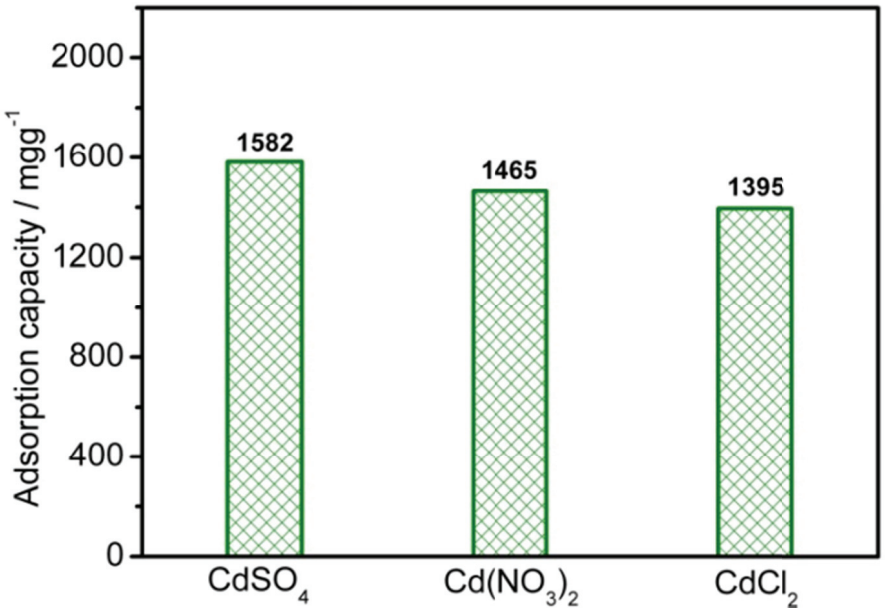

Fig.S23 Effect of anions on the electrosorption capacity of BNO nanosheets ($600 mgL^{-1} Cd^{2+}$) at 1.2 V by CDI with a flowing rate of 50 mgL^{-1}.

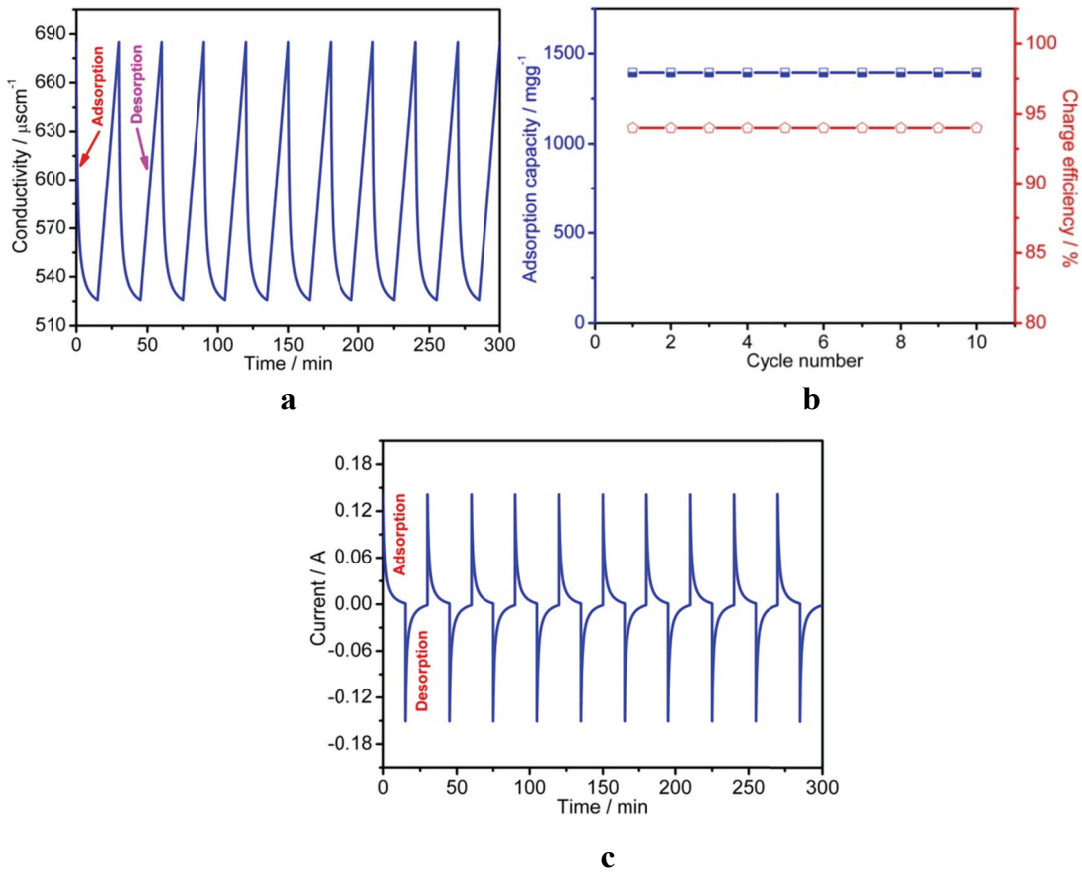

Fig.S24 (a) Solution conductivity changes; (b) electrosorption capacity and charge efficiencies; (c) the I–t curves of adsorption (charge at 1.2 V) and desorption (discharge at 0 V) for BNO nanosheets towards 600mgL^{-1} $CdCl_2$ aqueous solution at 1.2 V by CDI with a flowing rate of 50 mgL^{-1} over 10 cycles.

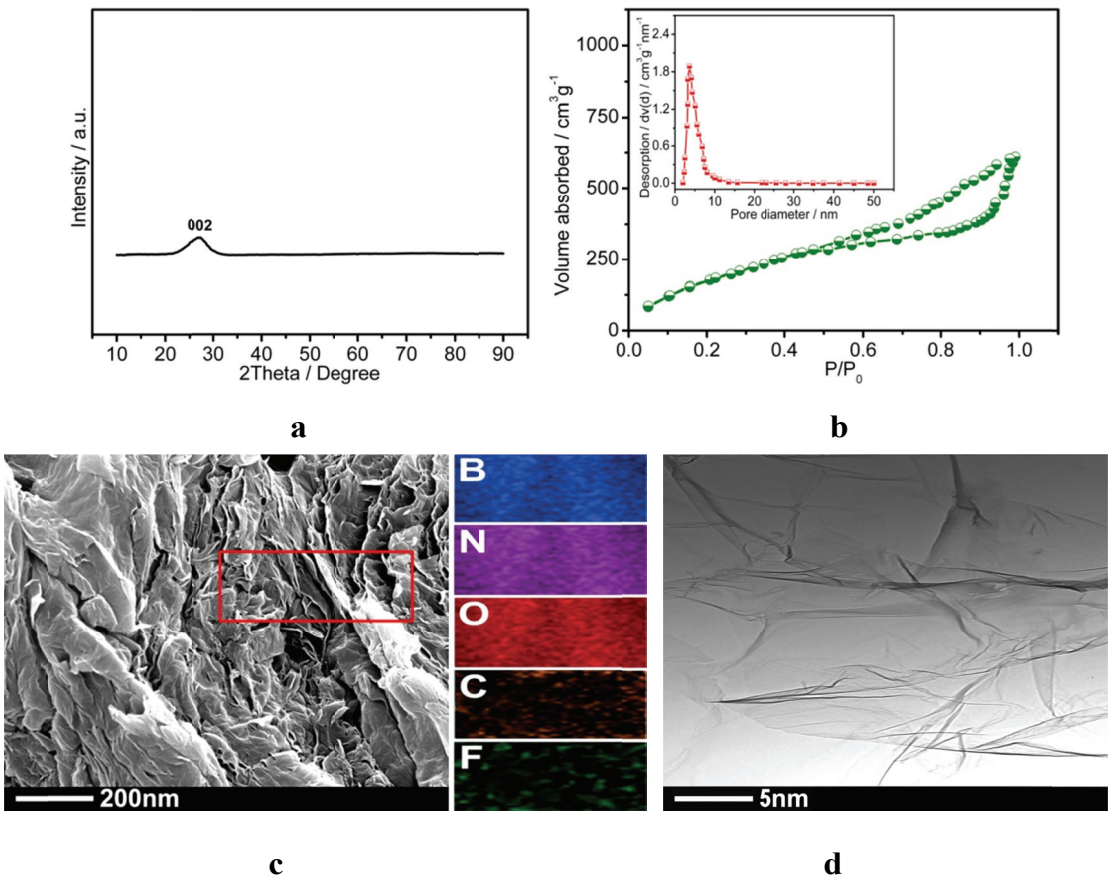

Fig.S25 (a) XRD profile; (b) Nitrogen sorption isotherm (the inset is the pore size distribution); (c) STEM image and the elemental mapping of its red frame (C and F elements originated from PTFE and carbon black) and (f) enlarged STEM image of the as-prepared BNO nanosheets after 10 cycles.

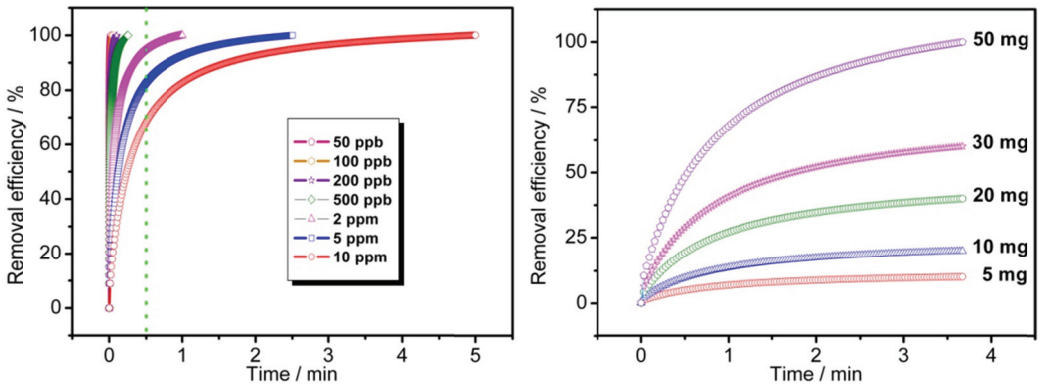

a **b**

Fig.S26 CDI Removal efficiency of (a)10 mg BNO nanosheets over Cd^{2+} 50 ppb to 10 ppm; (b) BNO nanosheets with different masses over 600 mgL^{-1} Cd^{2+} under 1.2 V at a flow rate of 50 mgL^{-1}.

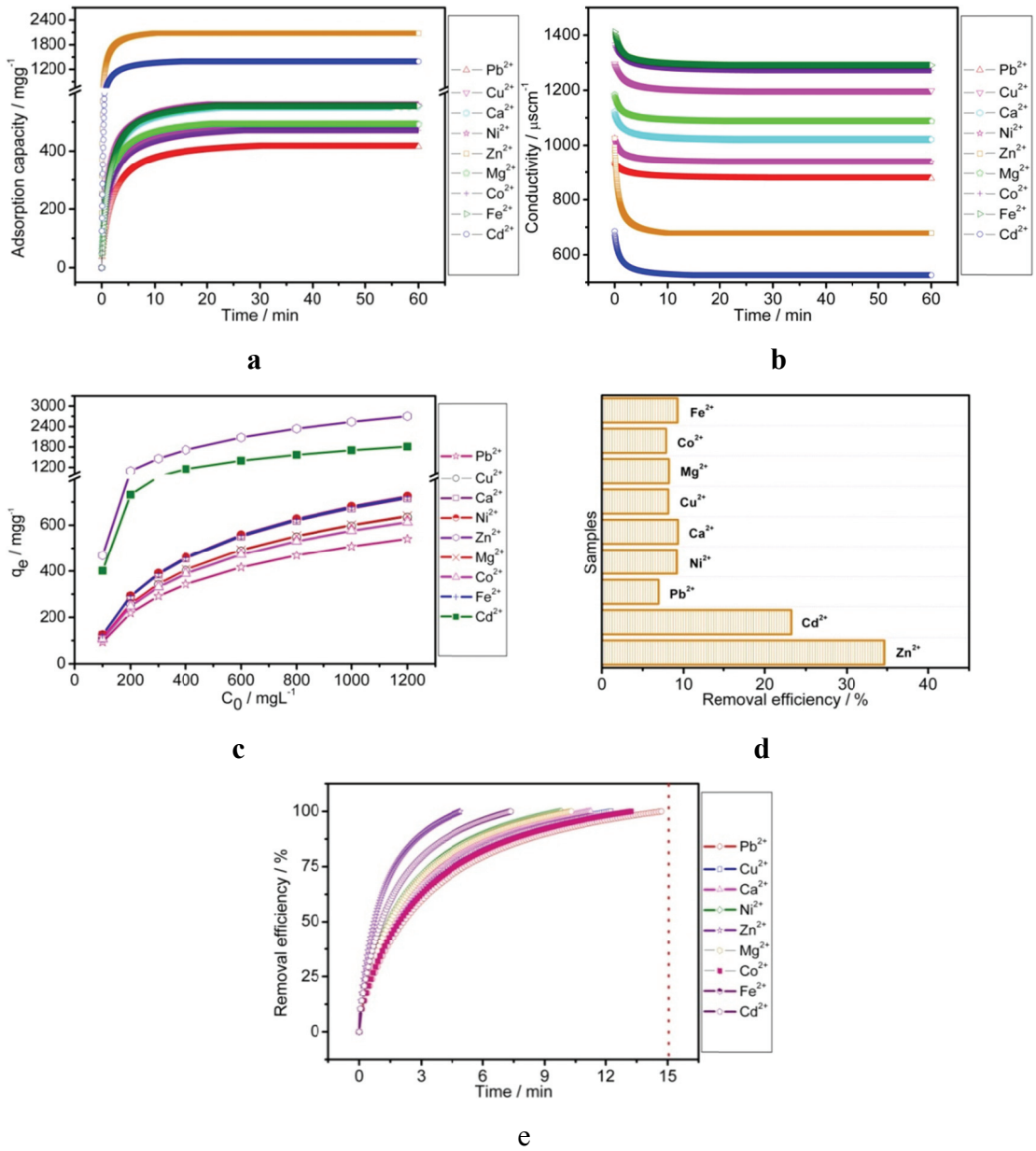

Fig.27 (a) In-situ electrosorption curves**;** (b) solution conductivity changes; (c) Electrosorption isotherms;(d) removal efficiency for individual metal ions in aqueous solution (600mgL^{-1}) over 10 mg BNO nanosheets; (e) Removal efficiency for competitive metal ions in 100 mL aqueous solution (600mgL^{-1}) on 200 mg BNO nanosheets at 1.2 V by CDI with a flowing rate of 50 mgL^{-1}.

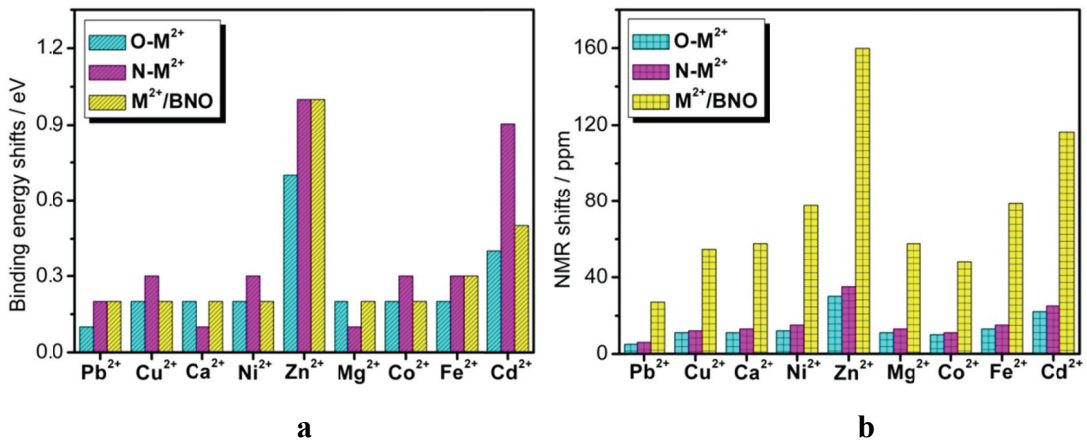

Fig.28 (a) Binding energy shifts of N, O and M^{2+} and (b) ^{15}N, ^{17}O and M^{2+} MAS NMR shifts of our BNO nanosheets after being charged at 1.2V in various meatl ions solution (600mgL^{-1}) at a flow rate of 50 mgL^{-1}. All the chemical shifts was detemined from the shifts of core peaks in the NMR spectra. The chemical shifts of Fe^{2+} and Ni^{2+} was detemined from their static NMR spectra.

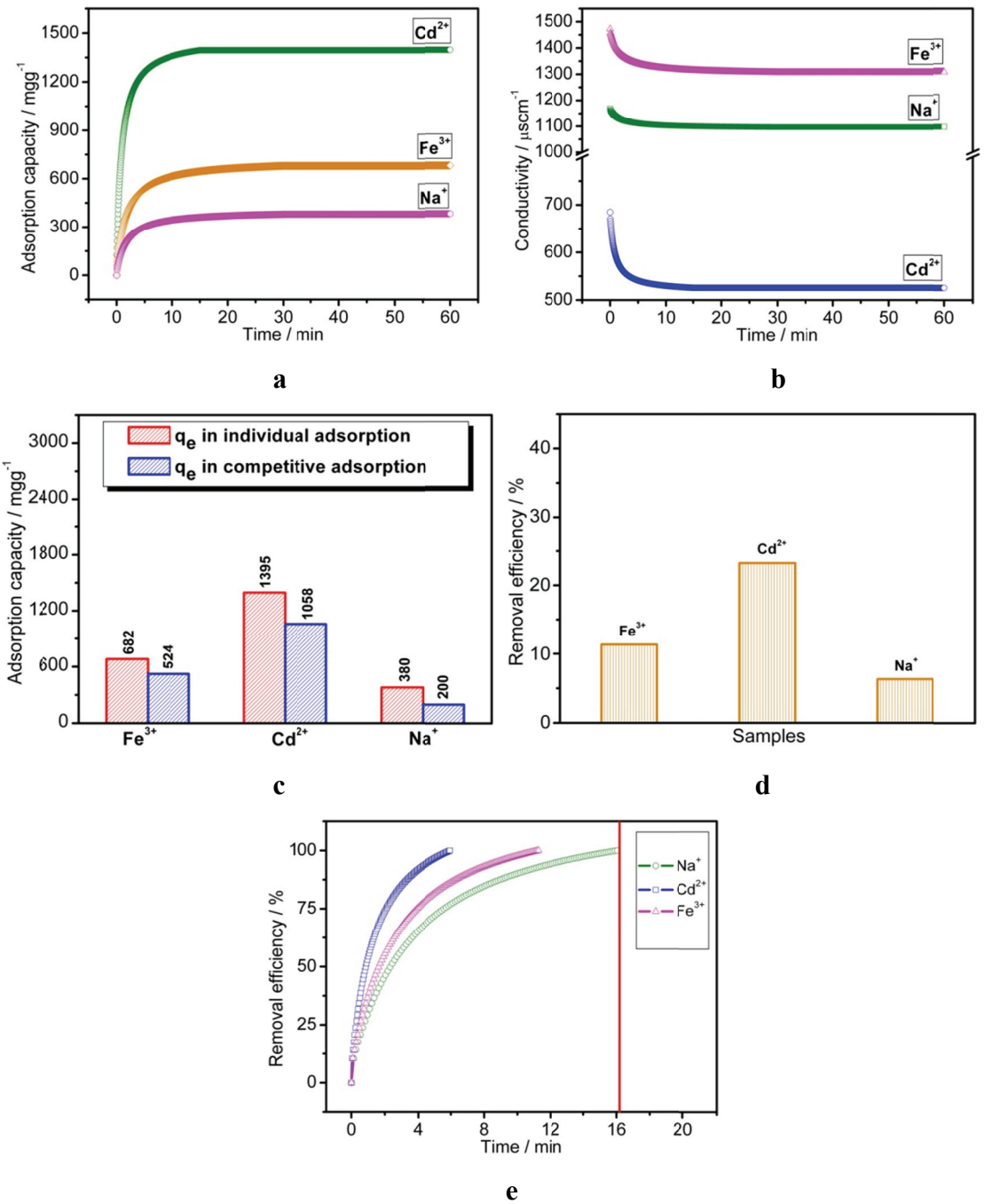

Fig.29 (a) In-situ electrosorption curves**;** (b) solution conductivity changes; (c) Electrosorption capacity in individual and competitive adsorption; (d) removal efficiency for individual metal ions in aqueous solution (600mgL^{-1}) over 10 mg BNO nanosheets; (e) Removal efficiency for competitive metal ions in 100 mL aqueous solution (600mgL^{-1}) on 200 mg BNO nanosheets at 1.2 V by CDI with a flowing rate of 50 mgL^{-1}.

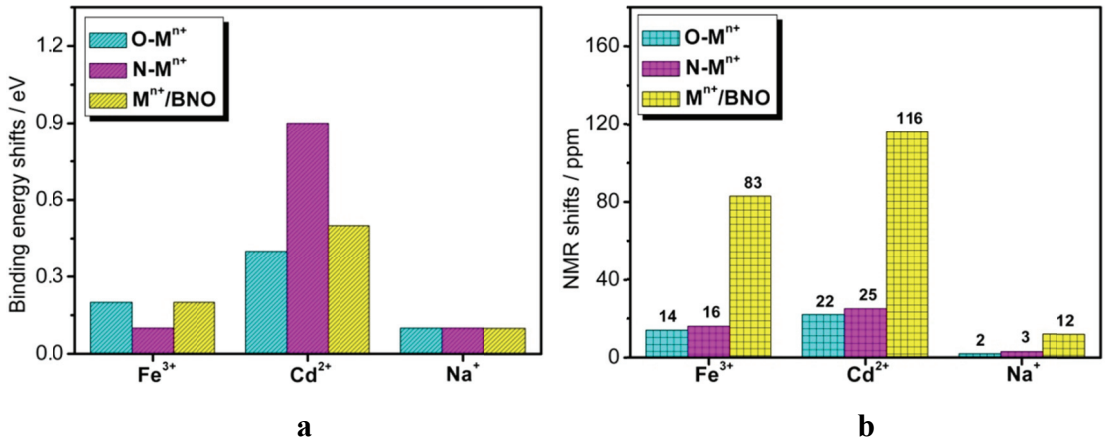

Fig.30 (a) Binding energy shifts of N, O and M^{n+} and (b) ^{15}N, ^{17}O and M^{n+} MAS NMR shifts of our BNO nanosheets after being charged at 1.2V in various meatl ions solution (600mgL^{-1}) at a flow rate of 50 mgL^{-1}. All the chemical shifts was detemined from the shifts of core peaks in the NMR spectra. The chemical shifts of Fe^{3+} was detemined from its static NMR spectra.

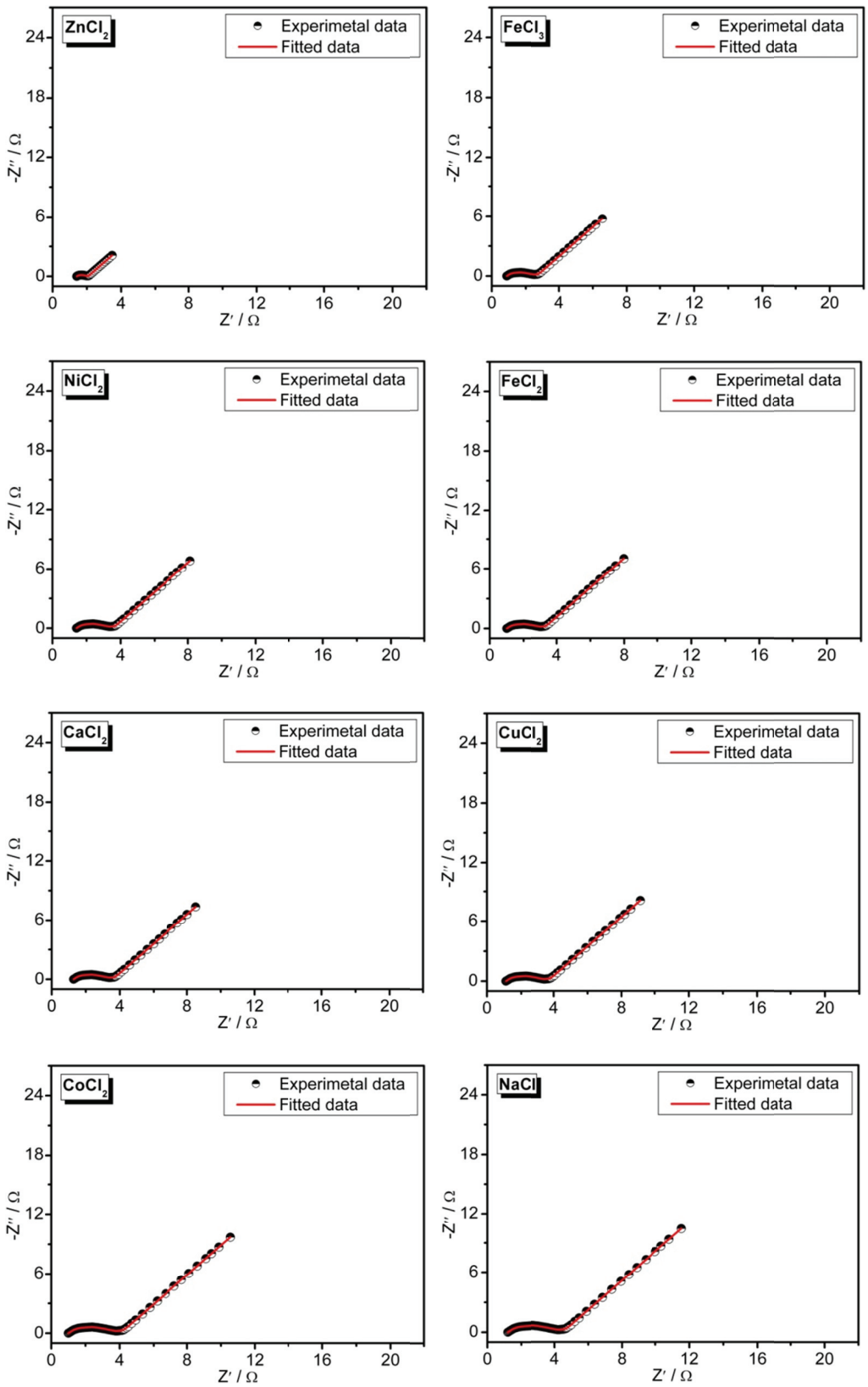
ZnCl2
FeCl3
NiCl2
FeCl2
CaCl2
CuCl2
CoCl2
NaCl
Experimetal data
Fitted data
-Z'' / Ω
Z' / Ω

(Continuted)

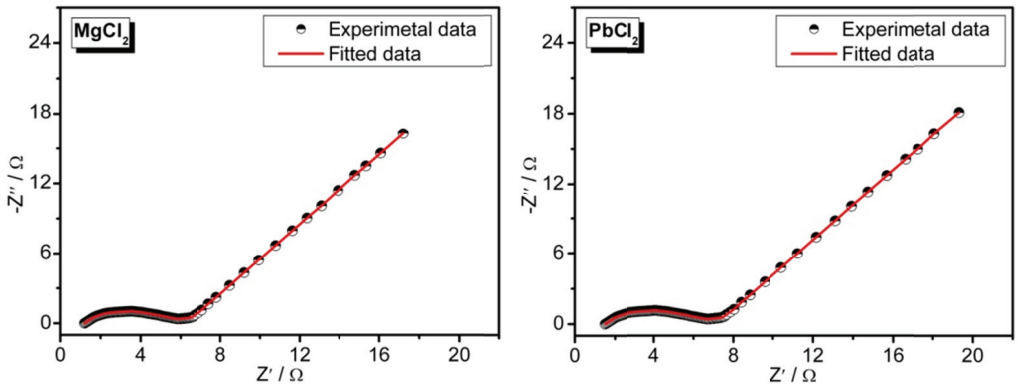

Fig.S31 Nyquist plots of the as-prepared BNO nanosheets in different ion solutions ($600mgL^{-1}$) at room temperature.

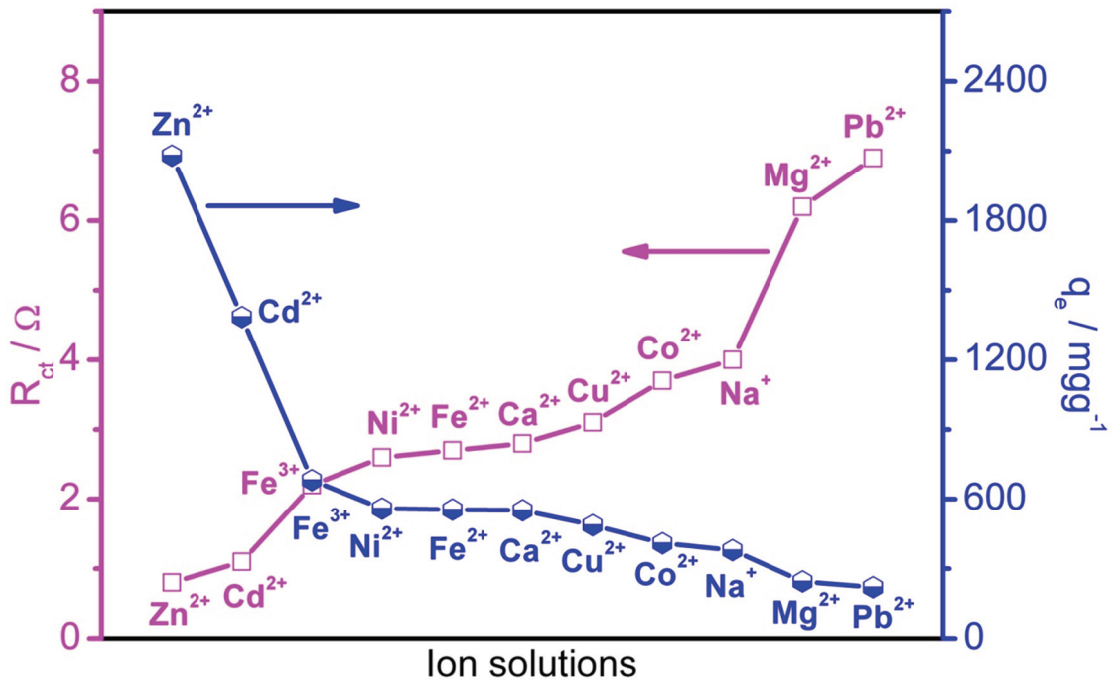

Fig.S32 The relationships between R_{ct} and q_e of BNO nanosheets being charged at 1.2V in various meatl ions solution (600mgL^{-1}) with a flow rate of 50 mgL^{-1}.